frontiers in Earth Science

ORIGINAL RESEARCH
published: 12 June 2020
doi: 10.3389/feart.2020.00167

A Global Assessment of Copper, Zinc, and Lead Isotopes in Mineral Dust Sources and Aerosols

Nina J. Schleicher[1], Shuofei Dong[1,2], Hollie Packman[1], Susan H. Little[1,3], Raquel Ochoa Gonzalez[1,4], Jens Najorka[5], Youbin Sun[6] and Dominik J. Weiss[1,7]**

[1] Department of Earth Science and Engineering, Imperial College London, London, United Kingdom, [2] Agilent Technologies Co. Ltd (China), Beijing, China, [3] Department of Earth Sciences, University College London, London, United Kingdom, [4] FICYT, Unit of European Projects, Foundation for the Promotion of Applied and Scientific Research of Asturias, Oviedo, Spain, [5] Core Research Departments, The Natural History Museum, London, United Kingdom, [6] State Key Laboratory of Loess and Quaternary Geology, Chinese Academy of Sciences, Xi'an, China, [7] Civil and Environmental Engineering, Princeton University, Princeton, NJ, United States

The stable isotope compositions of Cu and Zn in major geochemical reservoirs are increasingly studied with the aim to develop these isotope systems as tools to investigate the global biogeochemical cycles of these trace metals. The objectives of the present study were (i) to expand the range of Cu, Zn, and Pb isotope compositions of mineral dust by analyzing samples from major mineral dust sources in Asia and Africa (Chinese Loess Plateau, Chinese deserts, Thar desert, Sahel region) and (ii) to assess the potential impact of human activities on the isotope composition of aerosols by synthesizing published Cu and Zn isotope compositions in aerosols and natural and anthropogenic sources. For the newly analyzed mineral dust areas in Asia and Africa, $\delta^{65}Cu_{NIST-976}$ values range from −0.54 to +0.52‰, $\delta^{66}Zn_{JMC-Lyon}$ values from −0.07 to +0.57‰, and $^{206}Pb/^{204}Pb$ values from 18.522 to 19.696. We find a significant geographic control with samples from the Thar Desert having the heaviest isotopic compositions ($\delta^{65}Cu_{NIST-976}$ = +0.48 ± 0.06‰, $\delta^{66}Zn_{JMC-Lyon}$ = +0.49 ± 0.11‰) and samples from the Sahel and the Badain Jaran desert having the lightest Zn isotope composition ($\delta^{66}Zn_{JMC-Lyon}$ = +0.19 ± 0.15‰ and +0.07 ± 0.07‰, respectively). We find important variations in the isotope signatures between particle size fractions with heavier isotopic compositions in the smallest and largest particle size fractions and lighter isotopic compositions in the mid particle size fractions. Associations with the mineralogical composition are less clear. Newly analyzed aerosol samples for Beijing and Xi'an show $\delta^{65}Cu_{NIST-976}$ values of +0.29 ± 0.19‰ and +0.16 ± 0.04‰, $\delta^{66}Zn_{JMC-Lyon}$ values of −0.36 ± 0.04‰ and +0.02 ± 0.06‰, and $^{206}Pb/^{204}Pb$ values of 18.129 ± 0.003 and 18.031 ± 0.003, respectively. Based on a synthesis of published and novel data, we suggest improved ranges and mean values for the isotopic composition of mineral dust from selected locations in Asia and Africa and of anthropogenic sources such as non-exhaust traffic emissions, combustion, electroplating and galvanization. This should serve as a valuable reference for future studies using these isotope systems. This paper demonstrates univocally that human activity introduces a wide range of Zn isotope compositions into the atmospheric environment and, thus, impacts the biogeochemical cycle of Zn.

Keywords: isotopes, mineral dust, urban aerosols, anthropogenic, sources, MC-ICP-MS

OPEN ACCESS

Edited by:
Julia Ribeiro, Guangzhou Institute of Geochemistry (CAS), China

Reviewed by:
Luke Bridgestock, University of Oxford, United Kingdom
Shui Jiong Wang, China University of Geosciences, China

****Correspondence:***
Nina J. Schleicher
n.schleicher@imperial.ac.uk;
nina.j.schleicher@gmail.com
Dominik J. Weiss
d.weiss@imperial.ac.uk

Specialty section:
This article was submitted to Geochemistry, a section of the journal Frontiers in Earth Science

Received: *21 August 2019*
Accepted: *30 April 2020*
Published: *12 June 2020*

Citation:
Schleicher NJ, Dong S, Packman H, Little SH, Ochoa Gonzalez R, Najorka J, Sun Y and Weiss DJ (2020) A Global Assessment of Copper, Zinc, and Lead Isotopes in Mineral Dust Sources and Aerosols. Front. Earth Sci. 8:167. doi: 10.3389/feart.2020.00167

INTRODUCTION

Earth system processes and human activity influence the global biogeochemical cycles of copper (Cu) and zinc (Zn) in a variety of ways. For example, atmospheric long-range transport and deposition of mineral dust and particulate matter delivers these micronutrients to remote marine and terrestrial regions, controlling ecosystem development, and hence influencing the global carbon cycle (Mahowald et al., 2005). However, both metals are toxic at higher concentrations for oceanic microorganisms or when inhaled by humans, they induce adverse health effects. Zinc is associated with oxidative stress, which is a contributing factor in many chronic diseases (Prasad et al., 2004). Adamson et al. (2000) reported that the soluble Zn concentration in atmospheric dust determined the acute toxicity and caused inflammation of lung cells. Copper causes damage to molecules such as proteins and lipids (Brewer, 2010). Both Cu and Zn in urban atmospheric particles (Beijing) are present to a high percentage in easily leachable fractions and may therefore be environmentally mobile and bioavailable (Schleicher et al., 2011). Identifying their sources in atmospheric aerosols remains therefore critical for controlling emissions and improving air quality in urban environments (Moffet et al., 2008).

Trace metals in aerosols originate from anthropogenic and natural sources. Natural sources include soil and mineral dust particles, volcanic dust and gas, and biogenic particles (e.g., Moreno et al., 2009; Duan and Tan, 2013). Desert winds aerosolize several billion tons of soil-derived dust each year, including concentrated seasonal pulses from Africa and Asia (Kellogg and Griffin, 2006) and, consequently, natural reservoirs are important sources for aerosol particles. Even urban aerosols can be composed of a large proportion of mineral particles. In northern Chinese cities, including the capital Beijing, mineral dust particles play an important role especially in spring during so-called "Asian dust storms" (e.g., Mori et al., 2003; Xie et al., 2005; Schleicher et al., 2010, 2011; Sun et al., 2010; Yu et al., 2011; Chen et al., 2016). Asian dust plays also an important role on a global scale. For example, Uno et al. (2009) showed that Asian dust was transported one full circle around the globe. Ferrat et al. (2013) calculated dust fluxes numerically and estimated annual emissions of 179 Mt/y from Chinese dust sources. Xuan and Sokolik (2002) calculated annual mean PM_{10} emission rates that are ∼0.38 t/ha for the Taklimakan Desert, 0.24 t/ha for the Central Gobi Desert, and 0.05 t/ha for the deserts located on the Alxa Plateau. They calculated an annual mean dust emission of PM_{10} of 8.4 million tons. More than half of the total annual dust is emitted in spring (Xuan and Sokolik, 2002).

Examples of anthropogenic aerosol sources include emissions from fossil fuel combustion (largely used in energy production), industrial processes, domestic heating and cooking, exhaust and non-exhaust traffic sources like brake and tire abrasion, re-suspension, construction sites, and biomass burning (e.g., Moreno et al., 2009; Colbeck and Lazaridis, 2010; Calvo et al., 2013; Fuzzi et al., 2015). The chemical complexity and variability of the inorganic urban aerosol cocktail implies that the air pollution signature for each city needs to be individually characterized (Moreno et al., 2006) and that we need appropriate tools to fully trace the respective sources. However, source identification remains a challenging task because the methods developed so far (largely based on multivariate statistics) are often inconclusive and expensive (computationally and analytically).

A promising alternative is to use the stable isotope signatures of metals as a source apportionment tool. Variations in the isotopic composition of elements are widely used to identify and quantify source contributions and geochemical processes, which in turn improves our understanding of their biogeochemical cycles. Limitations in mass spectrometer designs, however, restricted the application of this approach to radiogenic and light stable elements until the development of multiple collector inductively coupled plasma source mass spectrometry (MC-ICP-MS) (e.g., Wiederhold, 2015). With respect to Cu and Zn, work on exploring their isotope systematics has focussed in particular on biogeochemical cycling in the aqueous environment (Maréchal et al., 2000; Vance et al., 2008; Peel et al., 2009; Little et al., 2014; Zhao et al., 2014; Moynier et al., 2017). Zhu et al. (2002) studied different mass fractionation processes of Cu isotopes (e.g., at high temperatures, redox-related, and biological processes). Other studies on Cu isotopes focussed on sulfides and hydrothermal mineralization (e.g., Ehrlich et al., 2004; Mason et al., 2005; Markl et al., 2006) while Zn isotopic ratios were utilized to identify pollutant sources first assessing dust pollution around a mining site in Siberia (Dolgopolova et al., 2006) and later in the River Seine (Chen et al., 2008). Subsequent work analyzed Zn isotope compositions of atmospheric particulates to assess the influence of industrial processes on isotope fractionation (Borrok et al., 2010; Ochoa Gonzalez and Weiss, 2015; Dong et al., 2017). Central to the efforts of using non-traditional stable isotopes for anthropogenic source tracing is the isotopic characterization of potential source materials and an improved understanding of what controls isotope variability at the source and along the pathway to the sink. This includes the effects of mineralogy and particle size fraction (Feng et al., 2009; Ferrat et al., 2011), atmospheric processing (Rubasinghege et al., 2010) and admixing of other sources during atmospheric transport (Ferrat et al., 2013).

Anthropogenic emissions have surpassed natural emissions for many trace elements (Rauch and Pacyna, 2009). This has affected the global atmospheric cycles of these elements and led to the atmospheric deposition in even the most remote areas (Marina-Montes et al., 2020). Anthropogenic processing can induce redox changes for metals that usually occur only in one oxidation state in the environment (Wiederhold, 2015). For example, ore smelting and roasting, the production of elemental metals, or engineered nanoparticles for industrial purposes, and combustion processes can cause isotope fractionation due to redox effects (including Zn), which may be preserved if the process is incomplete and isotopically fractionated metal pools with different oxidation states are released into the environment (Sonke et al., 2008; Mattielli et al., 2009). The main fractionation processes affecting the Zn isotope composition of atmospheric emissions are likely evaporation–condensation processes (Cloquet et al., 2008). The isotopic characterization of anthropogenic atmospheric endmembers

has been attempted in several studies, mostly for Zn but also for Cu.

The present study examines associations between observed isotopic compositions in urban aerosols and source reservoirs including mineral dust and anthropogenic materials. We first determine Cu, Zn, and Pb isotope compositions from a new set of major global mineral dust sources in Asia (Chinese Loess Plateau, Chinese deserts, and Thar desert) and Africa (Sahel region) to better characterize the range of isotopic compositions of this natural aerosol source and to assess the importance of geographic variability. We also present new isotope data of size-fractionated mineral dust samples to assess relevance of particle size to aerosol tracing. We then compile from published literature Zn and Cu isotope compositions of possible source materials in aerosols derived from human activity. The main emphasis is on Zn since more Zn isotope studies of anthropogenic materials are published. Finally, we compare isotopic compositions of urban aerosols (data from literature and novel data for two Chinese cities, Beijing and Xi'an) and of major natural and anthropogenic reservoirs to discuss implications for aerosol source tracing.

MATERIALS AND METHODS

Location and Description of Samples

We studied a set of mineral dust collected from major global dust sources. **Table 1** details the sampling sites of the mineral dust sources considered in this study: The Taklimakan desert of northwestern China (samples TK-074 and TK-103), the Tengger desert (TG-018), the Badain Jaran desert (BJ-024), and the Chinese Loess Plateau of northern China (CLS-20–90 and JY-1), the Thar desert of northwestern India (TDSD 1–3) and the Sahel region between Bamako and Timbuktu (SHD 10–32).

Four samples from the Chinese deserts (TG-018, BJ-024, TK-103, and TK-074) were separated into five size fractions by wet sieving (32–63 μm and >63 μm) and settling in solution [pipette method, see Lerman et al. (1974)] based on Stoke's Law (<4 μm, 4–16 μm, and 16–32 μm). Isotope ratios were determined in all fractions. Concentrations were determined in the lowest, highest and middle size fraction only due to sample limitations. Bulk isotopic compositions and concentrations of the samples were then calculated by mass balance with the concentrations of the missing size fractions approximated by taking the average concentrations of the size fractions above and below.

Two urban aerosol samples were collected in Xi'an and Beijing, China, during the summer of 2011. These samples were collected using the wet collection method [see Yan et al. (2015) for more details]. In Beijing, the collecting devices were placed on the roof (∼35 m above ground) of the Chinese Academy of Sciences, a building surrounded by mixed commercial and residential districts. In Xi'an, collecting devices were placed on the roof (∼45 m above ground) of a building in a residential district.

Sample Digestion of Mineral Dust and Aerosol Samples

All samples were digested in ISO 5 (class 100) laminar flow hoods in ISO 6 (class 1000) clean laboratories using previously developed methods (Ferrat et al., 2012b; Dong et al., 2013). All acids used were of supra-pure grade (HF) or purified by quartz distillation system (HNO_3 and HCl). Dilute solutions of acids were prepared with 18.2 MΩ cm^{-1} grade Millipore system (Bedford, USA). Laboratory equipment was cleaned with 6 M HCl, 15.4 M HNO_3 and distilled 0.5 M HNO_3 on a hot plate at 120°C for 24 h. Approximately 50 mg of each sample was digested using 1 ml of 24 M HF and 0.25 ml of 15.4 M HNO_3 in PFA vessels (Savillex, USA). The samples were digested on a hot plate at 150°C for 72 h. Every 24 h, the samples were put into an ultrasonic bath for 15 min. The samples were dried and re-dissolved twice in 0.5 ml 15.4 M HNO_3 and once in 0.5 ml 7 M HCl, to remove possible HF remaining in the digested samples. Samples were finally taken up in 3 ml 7 M HCl and separated into aliquots for concentration and isotope ratio analysis.

Determination of Cu, Zn, Pb, and Sc Concentrations and of Enrichment Factors

Concentrations of Cu, Zn, Pb, and Sc were determined by quadrupole inductively coupled plasma mass spectrometry (ICP-MS, Varian, USA; Ferrat et al., 2012b). Sample solutions were dried and re-dissolved in 10 ml 0.5 M HNO_3. External calibration solutions (0.1–200 $\mu g l^{-1}$ in 0.3 M HNO_3) were prepared by diluting multi-elemental standard solutions CCS-1 (Inorganic Ventures Inc.) containing 100 $mg l^{-1}$ Sc and CCS-6 including 100 $mg l^{-1}$ Pb, and single element Rb standard (VWR Aristar® 10,000 $mg l^{-1}$). Internal standard solutions were prepared using 1,000 $mg l^{-1}$ Rh and In (Alfa Aesar Specpure®) standard solutions. The limits of quantification were calculated after each run based on the intensity and standard deviation measurements of the calibration standards and calibration blank and were generally at or below a few tens of ng g^{-1} for Pb, Sc, Cu, and Zn. These were at least two orders of magnitude below the lowest concentrations measured. Accuracy and precision were based on repeat measurements of the certified reference material USGS G-2 granite. Repeat measurements ($n = 6$) showed a precision of 10% at 2σ-level for all analyzed elements. Copper, Zn, Pb, and Sc concentration were ∼6% lower than the certified values. Elemental concentrations for Cu and Zn in TK-074 and TK-103 were published previously as a part of the validation process for our improved analytical procedure (Dong et al., 2013).

The elemental enrichment factor (EF) was calculated using

$$EF = \frac{\left(\frac{X}{Sc}\right)_{sample}}{\left(\frac{X}{Sc}\right)_{ucc}} \quad (1)$$

where X is the element assessed, scandium (Sc) the reference element, and the upper continental crust (ucc) is the reference reservoir (Taylor and McLennan, 1985).

International Reference Standards and Standard Conversion

The variation of stable isotope ratios in nature is small. The small differences are expressed as delta values (δ) in per mill deviation

TABLE 1 | Sample ID, area of origin, and information on location of the mineral dust samples.

Sample ID	Area	Latitude	Longitude	Elevation
TG-018	Tengger Desert	39°00'22.4"N	103°34'01.7"E	1,304 m
BJ-024	Badain Desert	39°17'55.2"N	101°52'24.6"E	1,611 m
TK-074	Taklimakan Desert	41°64'43.3"N	83°29'01.5"E	1,001 m
TK-103	Taklimakan Desert	36°48'12.3"N	82°16'08.3"E	1,720 m
CLS-25	Loess Plateau	35°45'00"N	107°49'00"E	1,250 m
CLS-27	Loess Plateau	35°45'00"N	107°49'00"E	1,250 m
CLS-29	Loess Plateau	35°45'00"N	107°49'00"E	1,250 m
CLS-90	Loess Plateau	35°33'00"N	107°27'00"E	1,250 m
CLS-20	Loess Plateau	35°33'00"N	107°27'00"E	1,205 m
MG-09022	Southern Mongolia	43°44'07.5"N	107°22'35.8"E	1,449 m
JY-1 (<16 μm)	Loess samples	Jingyuan profile		3.5 m
JY-1 (16-63 μm)	Loess samples	Jingyuan profile		
TDSD-01	Thar Desert	Figure 1 in (Ferrat et al., 2011)		
TDSD-02	Thar Desert	Figure 1 in (Ferrat et al., 2011)		
TDSD-03	Thar Desert	Figure 1 in (Ferrat et al., 2011)		
SHD-10	Sahel Desert	Between Bamako and Timbuktu		
SHD-18	Sahel Desert	Between Bamako and Timbuktu		
SHD-21	Sahel Desert	Between Bamako and Timbuktu		
SHD-32	Sahel Desert	Between Bamako and Timbuktu		

from a reference according to

$$\delta = (\frac{R_{sample}}{R_{ref}} - 1)^{*}1000 \quad (2)$$

where R_{sample} and R_{ref} are the sample and reference isotope ratios, respectively.

The referencing standards used during measurement sessions in individual laboratories are so called "in-house" or working standards and differ from laboratory to laboratory. Consequently, for inter-comparison, δ-values expressed relative to a working standard need to be converted and reported relative to an international reference standard. The δ-value for a sample (δ_{sample}) measured against a working standard (δ_{work}) on an international scale (δ_{ref}) [see Werner and Brand (2001)] is given by

$$\delta_{sample/ref} = \delta_{Sample/work} + \delta_{work/ref} + \delta_{sample/work}\, x\, \delta_{work/ref}/1000. \quad (3)$$

For Zn, four standards have to date been widely used and hence can essentially serve as an "international" reference standard: (i) the Johnston and Matthew JCM 3-0749L single element solution (called "JMC-Lyon") from the ENS Lyon (denoted thereafter as JMC-Lyon standard, Maréchal et al., 1999); (ii) the IRMM-3702 certified isotope standard produced by the Institute for Reference Materials and Measurements (IRMM) in Belgium (denoted as IRMM standard); (iii) the AA-ETH single element solution from the ETH Zürich (denoted as AA-ETH standard, Archer et al., 2017) and (iv) the SRM-683 standard from NIST. The International Atomic Energy Agency (IAEA) recommends using in-house working standard materials instead of international standards during measurements on a daily basis (Werner and Brand, 2001). Arguments including similar properties of the sample and the standard, homogeneity, available quantities, costs for which primary reference material to use as an international standard have been widely discussed (e.g., Brand et al., 2014; Archer et al., 2017; Moynier et al., 2017) and conversion values based on intercalibration efforts (Moeller et al., 2012; Archer et al., 2017) or statistical analysis of published values (Moynier et al., 2017) were proposed. To date, no complete summary of all measured Zn standard values has been presented so we compiled these published values for the different Zn standards in **Table 2**.

We report δ-values relative to the Lyon standard ($\delta^{66}Zn_{JMC-Lyon}$). The rationale was that most of the data used in this study were originally measured against the Lyon standard, hence conversions were kept to a minimum. Furthermore, the majority of publications still report Zn isotope variations relative to the Lyon standard. We used the following conversions values for $\delta^{66}Zn_{IRMM-3702}$, $\delta^{66}Zn_{AA-ETH}$, and $\delta^{66}Zn_{SRM-683}$:

Standard:	$\delta^{66}Zn_{JMC-Lyon}$ (‰):	Reference:
IRMM-3702	+0.29	Average of 24 studies compiled in **Table 2**
AA-ETH	+0.28	(Archer et al., 2017)
SRM-683	+0.12	(Yang et al., 2018)

Figure 1 displays the relative location of $\delta^{66}Zn$ of the suggested standards (IRMM-3702, AA-ETH, SRM-683) vs. JMC-Lyon. Exemplarily, we added two generic samples A and B to this graph to illustrate the $\delta^{66}Zn$ location relative to IRMM and Lyon (see blue solid and red dashed arrows), respectively, to avoid wrong conversions.

TABLE 2 | $\delta^{66}Zn_{JMC-Lyon}$ values of different international standard materials.

Standard	References	$\delta^{66}Zn_{JMC-Lyon}$	±2σ	*n*
IRMM-3702	Cloquet et al. (2006)	0.32	0.16	2
	Petit et al. (2008)	0.32	0.03	4
	Borrok et al. (2010)	0.27	0.07	24
	Moeller et al. (2012)	0.29	0.05	5
	Aranda et al. (2012)	0.31	0.01	12
	Deng et al. (2014)	0.28	0.05	27
	Sossi et al. (2015)	0.30	0.02	10
	Aebischer et al. (2015)	0.27	0.07	23
	Araújo et al. (2016)	0.27	0.07	30
	Doucet et al. (2016)	0.27	0.02	4
	Guinoiseau et al. (2016)	0.28	0.03	14
	Moynier et al. (2017)	0.30	0.06	163
	Moore et al. (2017)	0.32	0.06	10
	Nelson et al. (2017)	0.25	0.11	
	Wang et al. (2017)	0.27	0.03	50
	Araújo et al. (2018)	0.27	0.06	30
	Doucet et al. (2018)	0.28	0.02	24
	Yin et al. (2018)	0.31	0.04	18
	Zhang et al. (2018)	0.25	0.04	30
	Dinis et al. (2018)	0.27	0.05	12
	Debret et al. (2018)	0.30	0.04	
	Souto-Oliveira et al. (2019)	0.28	0.05	36
	Liu et al. (2019)	0.27	0.03	127
	Köbberich and Vance (2019)	0.30	0.06	163
	AVERAGE (*n* = 24 studies)	**0.29**		
SRM-683	Yang et al. (2018)	0.12	0.04	295
	Dinis et al. (2018)	0.12	0.04	19
AA-ETH	Archer et al. (2017)	0.28	0.02	110
	Nelson et al. (2017)	0.26	0.10	32

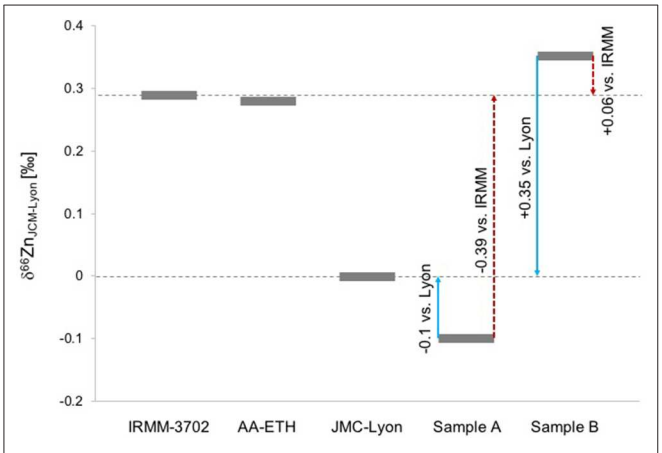

FIGURE 1 | Relative location of $\delta^{66}Zn_{JMC-Lyon}$ values of different international standards (IRMM-3702, AA-ETH, SRM-683) and the effect of conversion for generic samples A and B against IRMM-3702 or JMC-Lyon standards, respectively.

The widely used international reference material SRM-976 (elemental Cu) from NIST (denoted thereafter NIST-976) to report Cu isotope data is not anymore commercially available. Two European Reference Materials (ERM by the European Commission) standards (Cu nitrate solutions), ERM-AE-633 and ERM-AE-647 were recently proposed as new international standards (Moeller et al., 2012). The advantage of the ERM-AE-633 standard is that it has almost the same δ-value as the NIST-976 [variations of ±0.01 were reported by Moeller et al. (2012), Šillerová et al. (2017), Kříbek et al. (2018)] and it was proposed that no conversion between δ-values reported relative to AE-633 is necessary (Peréz Rodríguez et al., 2013; Kusonwiriyawong et al., 2017). We report all δ-values relative to the NIST-976 standard and use the following conversion values:

Standard:	$\delta^{65}Cu_{NIST-976}$ (‰):	Reference:
AE-633	±0	(Peréz Rodríguez et al., 2013)
AE-647	−0.21	(Moeller et al., 2012)

Isotope Ratio Determinations of Cu, Zn, and Pb

Prior to isotope ratio analysis, Cu, Zn, and Pb were separated from matrix elements using ion exchange chromatography procedures previously developed to account for small sample size, low concentrations, and complex matrices (Ferrat et al., 2012a; Dong et al., 2013). For Cu and Zn isotope ratio measurements, separation from elements such as Mg, V, Ti, Ni, Cr, and Ba is necessary because these elements generate interferences with Cu and Zn isotopes in argide form (Mg), (hydro)-oxide form (Cr, Ti, V), or double-charged species (Ba). A Bio-Rad AGMP-1 resin (100–200 mesh) was employed for the separation. To ensure complete separation from the matrix, the Cu fraction was passed through the ion exchange column twice and the Zn fraction once. We tested the yield for Zn and Cu during passage of ion exchange resin with an in-house granite (HRM-24) throughout the course of the study. The column recoveries for the HRM-24 granite were quantitative for both elements: 98 ± 5% for Zn ($n = 3$) and 96 ± 4% for Cu ($n = 3$). The Cu and Zn solutions were dried and re-dissolved in 0.1 ml 15.4 M HNO_3 and evaporated to remove the remaining chlorides and finally dissolved in 1 ml 0.1 M HNO_3 for isotope ratio analysis. For the Pb isotope ratio determinations, Pb was isolated with an EiChrom selective extraction Sr-resin following a previously developed procedure (Ferrat et al., 2012a).

A Nu plasma source multiple-collector mass spectrometer (MC-ICP-MS, Wrexham, UK) connected to a Nu DSN-100 Desolvation Nebulizer System was used for the isotope analysis. Instrumental mass bias effects were corrected using standard sample bracketing for Cu and double spike for Zn (Arnold et al., 2010). Zinc isotope ratios are reported against the "JCM-Lyon"-standard JCM 3-0749L and Cu isotope composition

against NIST-976 standard using the δ-notation:

$$\delta^{66}Zn_{JMC-Lyon} = \left(\frac{\left(\frac{^{66}Zn}{^{64}Zn}\right)_{sample}}{\left(\frac{^{66}Zn}{^{64}Zn}\right)_{JMC-Lyon}} - 1 \right) * 1000 \quad (4)$$

$$\delta^{65}Cu_{NIST-976} = \left(\frac{\left(\frac{^{65}Cu}{^{63}Cu}\right)_{sample}}{\left(\frac{^{65}Cu}{^{63}Cu}\right)_{NIST-976}} - 1 \right) * 1000 \quad (5)$$

The total procedural blank for Cu and Zn after separation was ∼3.5 and 5 ng, respectively. Accuracy and precision were monitored by repeated measurements of the geological standards BCR-027 Blend Ore and USGS-G2 granite and the industrial single element standards Romil Cu and Romil Zn. Within error, the isotope ratios of the reference materials were identical to previously reported values (see **Table S1**). Precision was estimated by the average analytical error (±2 sigma) of the mineral dust samples measured in this study, i.e., 0.07‰ for δ^{65}Cu- and 0.07‰ for δ^{66}Zn-values. Isotope data for Cu and Zn in TK-074 and TK-103 were published previously as a part of the validation process for our improved analytical procedure (Dong et al., 2013).

For the analysis of Pb isotope ratios, samples and the NIST-SRM 981 Pb standard were doped with NIST-SRM 997 Tl with the same ratio (Pb/Tl = 3:1) and to the same concentrations. Instrumental mass bias was corrected using Tl for mass bias corrections (Weiss et al., 2004). Precision and accuracy were assessed using repeated measurements ($n = 14$) of the USGS G-2 granite over the study period. Values of 18.414 ± 0.003, 15.633 ± 0.004, 38.893 ± 0.025 for ^{206}Pb/^{204}Pb, ^{207}Pb/^{204}Pb, and ^{208}Pb/ ^{204}Pb are within error in good agreement with previously published data (see **Table S1**). Selected Pb isotope data from the Thar desert (TDSD-01, TDSD-02, TDSD-03) and the Loess Plateau (CLS-20, CLS-25, CLS-27, CLS-29, CLS-90) were published previously (Ferrat et al., 2012a).

Mineralogical Determinations (XRD)

The mineral compositions of the samples were determined using X-ray diffraction (XRD). X-ray powder diffraction data were collected using an Enraf-Nonius PDS120 diffractometer equipped with a primary Germanium (111) monochromator and an INEL 120° curved position sensitive detector. The dust samples were ground in an agate mortar and loaded into a circular well-mount of 7 and 13.5 mm diameter with a depth of 1 mm. Operating conditions for the Cu source were 40 kV and 35 mA. The horizontal slit after the monochromator was set to 0.24 mm to confine the incident beam to pure Cu Kα1 radiation. The angular linearity of the detector was calibrated using the external standards silver behenate ($AgC_{22}H_{43}O_2$) and silicon (NIST SRM 640). The full 2-Theta linearization was performed with a least-squares cubic spline function. The whole pattern stripping method described in detail elsewhere (Cressey and Schofield, 1996) was used to derive the phase proportions. For mineral quantification, appropriate standards were selected from reference materials of the mineral collection at the Natural History Museum, London, and analyzed under identical run conditions as the samples. In some samples, total mineral composition was below 100 wt.%. This indicated the presence of amorphous components and minor amounts of unidentified phases where low-intense peaks could not be assigned to a phase. Quantification errors were assessed varying best-fit scale factors while inspecting the influence on the residual background. The estimated relative error for the mineral assemblages was 5 and 10% for phase proportions above and below 10 wt.%, respectively.

RESULTS

We present in this section the results of the new data set acquired for the samples collected from the Chinese, Indian and Saharan deserts.

Concentrations and Isotope Ratios of Bulk Mineral Dust

Elemental concentrations of mineral dust samples are lowest in the Sahel Region and Thar Desert and highest in the Chinese deserts (Tengger, Badain Jaran, Taklimakan, Gobi). Copper concentrations in the Thar Desert are up to 10 μg/g and in the Chinese deserts up to 69 μg/g, Zn concentrations in the Thar Desert are up to 35 μg/g and in the Chinese deserts up to 203 μg/g. By comparison, upper continental crust Cu and Zn concentrations are 28 and 67 μg/g, respectively (Rudnick and Gao, 2003). Lead concentrations in the Sahel Region are up to 16 μg/g and in the Chinese deserts up to 30 μg/g (**Table 3**).

The isotopic compositions of mineral dust samples (bulk and individual size fractions) range between −0.07‰ and +0.57‰ for $\delta^{66}Zn_{JMC-Lyon}$, between −0.54‰ and +0.52‰ for $\delta^{65}Cu_{NIST-976}$, and between 18.522 and 19.696 for ^{206}Pb/^{204}Pb (**Table 3**). The isotope ratios of the mineral dust samples from the different regions are shown in **Figure 2**. The $\delta^{66}Zn_{JMC-Lyon}$ values from samples of the Chinese deserts range between +0.07‰ and +0.33‰, of the Chinese Loess Plateau between +0.22‰ and +0.49‰, of the Thar desert between +0.41‰ and +0.57‰ and of the Sahel region between −0.02‰ and +0.31‰. The $\delta^{65}Cu_{NIST-976}$ values in the Chinese deserts range between 0.00‰ and +0.14‰, in the Chinese Loess Plateau between +0.16‰ and +0.38‰, in the Thar desert between +0.44‰ and +0.52‰ and in the Sahel region between −0.20‰ and +0.11‰. The ^{206}Pb/^{204}Pb in the bulk mineral dust from the Chinese Deserts range between 18.542 and 18.888, in the Chinese Loess Plateau between 18.731 and 18.832, in the Thar desert between 19.604 and 19.696 and in the Sahel region between 18.747 and 19.224.

Concentration and Isotope Ratios of Cu, Zn, and Pb in Particle Size Fractions

Copper concentrations decrease from the smallest to the largest fraction in samples from the Tengger desert (TG-018) and Badain Jaran desert (BJ-024) (**Table 3**). The samples from the Taklimakan desert (TK-074 and TK-103) have the lowest Cu concentration in the 16–32 μm size fraction. Zinc concentrations correlate inversely with particle size in all samples, with a range between 206 and 389 μg/g of Zn in the <4 μm size

TABLE 3 | Sample origin, sample ID, particle size fraction and distribution, elemental concentration, isotope ratios, and enrichment factors for the samples analyzed in this study.

	Comment	Sample ID	Particle size analysis		Concentrations				Isotope ratios										Enrichment factors	
			Fraction	Distribution	[Zn]	[Cu]	[Pb]	[Sc]	δ^{66}Zn (JMC-Lyon)	±2σ	δ^{65}Cu (NIST-976)	±2σ	^{206}Pb/^{204}Pb	±2σ	^{207}Pb/^{204}Pb	±2σ	^{208}Pb/^{204}Pb	±2σ	EF_{Zn}	EF_{Cu}
			µm	%	µg/g	µg/g	µg/g	µg/g	‰	‰	‰	‰								
Chinese deserts	Tengger	TG-018	<4	21.1	254	56	37	18	0.46	0.06	0.25	0.10	18.565	0.002	15.677	0.002	38.835	0.004	2.2	1.4
			4–16	27.9					0.23	0.06	−0.54	0.11	18.613	0.002	15.676	0.002	38.870	0.006		
			16–32	14.9	219	23	20	12	0.21	0.07	−0.06	0.09	18.772	0.001	15.682	0.001	38.972	0.002	2.8	0.9
			32–63	13.4					0.27	0.08	0.08	0.10	18.771	0.001	15.680	0.001	38.880	0.003		
			>63	22.7	43	11	14	7	0.28	0.06	0.43	0.09	18.634	0.002	15.679	0.002	38.827	0.005	1.0	0.7
			bulk		*160*	*28*	*24*	*12*	*0.31*	*0.06*	*0.00*	*0.10*	*18.653*		*15.678*		*38.869*			
	Badain Jaran	BJ−024	<4	29.5	206	52	31	19	0.19	0.09	0.17	0.14	18.563	0.001	15.648	0.001	38.719	0.004	1.7	1.2
			4–16	32.8					0.07	0.05	−0.31	0.12	18.614	0.001	15.651	0.001	38.786	0.002		
			16–32	12.7	214	28	19	12	−0.06	0.06	0.15	0.10	18.720	0.002	15.659	0.002	38.896	0.005	2.7	1.0
			32–63	6.8					−0.07	0.09	0.38	0.08	18.666	0.002	15.656	0.002	38.807	0.004		
			>63	18.3	73	20	14	7	−0.01	0.07	0.39	0.10	18.662	0.002	15.661	0.002	38.791	0.006	1.6	1.2
			bulk		*165*	*36*	*23*	*14*	*0.07*	*0.07*	*0.06*	*0.12*	*18.625*		*15.653*		*38.783*			
	Taklimakan	TK−074	<4	39.5	389	68	38	17	0.23	0.05	0.03	0.12	18.658	0.002	15.667	0.002	38.837	0.004	3.5	1.7
			4–16	40.9					0.14	0.08	−0.02	0.08	18.678	0.002	15.664	0.002	38.842	0.005		
			16–32	11.0	184	27	19	10	0.08	0.08	0.20	0.09	18.742	0.001	15.669	0.001	38.881	0.002	2.8	1.2
			32–63	4.1					0.17	0.09	−0.12	0.11	18.609	0.001	15.658	0.001	38.743	0.001		
			>63	4.5	41	86	12	nd	0.38	0.06	0.37	0.10	18.522	0.002	15.648	0.002	38.674	0.006		
			bulk		*203*	*52*	*30*	*nd*	*0.18*	*0.07*	*0.04*	*0.10*	*18.665*		*15.663*		*38.829*			
	Taklimakan	TK−103	<4	18.8	321	78	39	17	0.28	0.08	0.2	0.16	18.869	0.001	15.674	0.001	38.918	0.003	3.0	2.1
			4–16	32.5					0.14	0.04	0.31	0.10	18.888	0.001	15.675	0.001	38.950	0.004		
			16–32	24.6	147	21	17	10	0.13	0.05	0.06	0.12	18.995	0.002	15.683	0.002	39.128	0.007	2.2	0.9
			32–63	14.9					0.35	0.07	−0.06	0.09	18.787	0.002	15.671	0.002	38.942	0.006		
			>63	9.3	84	27	13	8	0.48	0.06	−0.07	0.09	18.805	0.001	15.669	0.001	38.859	0.001	1.6	1.4
			bulk		*144*	*34*	*24*	*12*	*0.23*	*0.06*	*0.14*	*0.11*	*18.888*		*15.676*		*38.978*			
	Gobi Desert	MG-09022	bulk		91	69	12	14	0.33	0.09	0.15	0.11	18.542	0.003	15.603	0.003	38.538	0.009	1.0	2.5
Chinese Loess Plateau		CLS-25	bulk		67	24	14	8	0.24	0.09	0.38	0.09	18.783	0.003	15.6681	0.002	38.960	0.009	1.3	1.4
		CLS-27	bulk		80	29	18	13	0.35	0.08	0.31	0.10	18.780	0.015	15.667	0.015	38.970	0.032	0.9	1.0
		CLS-29	bulk		80	29	19	14	0.32	0.08	0.16	0.11	18.789	0.024	15.670	0.014	39.006	0.053	0.9	0.9
		CLS-90	bulk		90	33	20	14	0.47	0.07		–	18.814	0.014	15.671	0.012	39.006	0.029	1.0	1.0
		CLS-20	bulk		65	25	14	9	0.49	0.07	0.23	0.09	18.832	0.015	15.673	0.014	38.961	0.053	1.1	1.2
	Jay Yuan	JY-1	<16	15.0	73	16	10	8	0.46	0.04	0.16	0.10	18.731	0.003	15.671	0.002	38.951	0.007	1.4	1.0
			16–63	82.5	140	30	19	12	0.22	0.04	0.16	0.10	18.827	0.002	15.675	0.001	39.038	0.004	1.8	1.2

(Continued)

TABLE 3 | Continued

	Comment	Sample ID	Particle size analysis		Concentrations				Isotope ratios										Enrichment factors	
			Fraction	Distribution	[Zn]	[Cu]	[Pb]	[Sc]	δ^{66}Zn (JMC-Lyon)	±2σ	δ^{65}Cu (NIST-976)	±2σ	^{206}Pb/^{204}Pb	±2σ	^{207}Pb/^{204}Pb	±2σ	^{208}Pb/^{204}Pb	±2σ	EF_{Zn}	EF_{Cu}
			μm	%	μg/g	μg/g	μg/g	μg/g	‰	‰	‰	‰								
Average (omitted JY-1)					*76*	*28*	*17*	*12*	*0.37*	*0.08*	*0.27*	*0.10*	*18.800*		*15.670*		*38.981*		1.1	1.1
Stdev					*10*	*3*	*3*	*3*	*0.11*	*0.01*	*0.10*	*0.01*	*0.022*		*0.002*		*0.024*			
Thar desert	Thar	TDSD-01	bulk		31	7	18	9	-	-	-	-	19.696	0.004	15.865	0.004	39.962	0.014	0.5	0.4
	Thar	TDSD-02	bulk		35	10	20	8	0.57	0.07	0.44	0.07	19.604	0.008	15.849	0.009	39.984	0.022	0.7	0.6
	Thar	TDSD-03	bulk		33	9	18	8	0.41	0.07	0.52	0.07	19.672	0.002	15.858	0.002	40.081	0.006	0.7	0.5
Average					*33*	*9*	*19*	*8*	*0.49*	*0.07*	*0.48*	*0.07*	*19.66*		*15.86*		*40.01*		0.6	0.5
Stdev					*2*	*2*	*1*	*1*	*0.11*	*0.00*	*0.06*	*0.00*	*0.05*		*0.01*		*0.06*		0.1	0.1
Sahel region	Mali	SHD-10	bulk		42	31	16	16	−0.02	0.04	0.09	0.04	19.037	0.009	15.762	0.008	39.836	0.007	0.4	0.8
	Mali	SHD-18	bulk		4	2	2	1	0.31	0.04	0.11	0.04	18.747	0.009	15.667	0.009	38.861	0.035	0.8	0.9
	Mali	SHD-21	bulk		5	2	2	1	0.24	0.04	−0.04	0.04	18.955	0.013	15.692	0.011	39.067	0.032	0.9	1.2
	Mali	SHD-32	bulk		6	3	3	2	0.23	0.04	−0.20	0.04	19.224	0.010	15.741	0.008	39.468	0.034	0.5	0.8
Average (omitted SHD-10)					*4.95*	*2.31*	*2.45*	*1.12*	*0.26*	*0.04*	*−0.04*	*0.04*	*18.98*		*15.70*		*39.13*		0.7	1.0
Stdev					*1.06*	*0.73*	*0.65*	*0.55*	*0.04*	*0.00*	*0.15*	*0.00*	*0.24*		*0.04*		*0.31*			
Aerosols	Xi'an	XA324	bulk		475	34	31	11	0.02	0.06	0.16	0.04	18.031	0.003	15.588	0.003	38.284	0.006	6.9	1.5
	Beijing	BJ324	bulk		70	25	16	9	−0.36	0.04	0.29	0.19	18.129	0.003	15.585	0.004	38.274	0.010	1.3	1.4

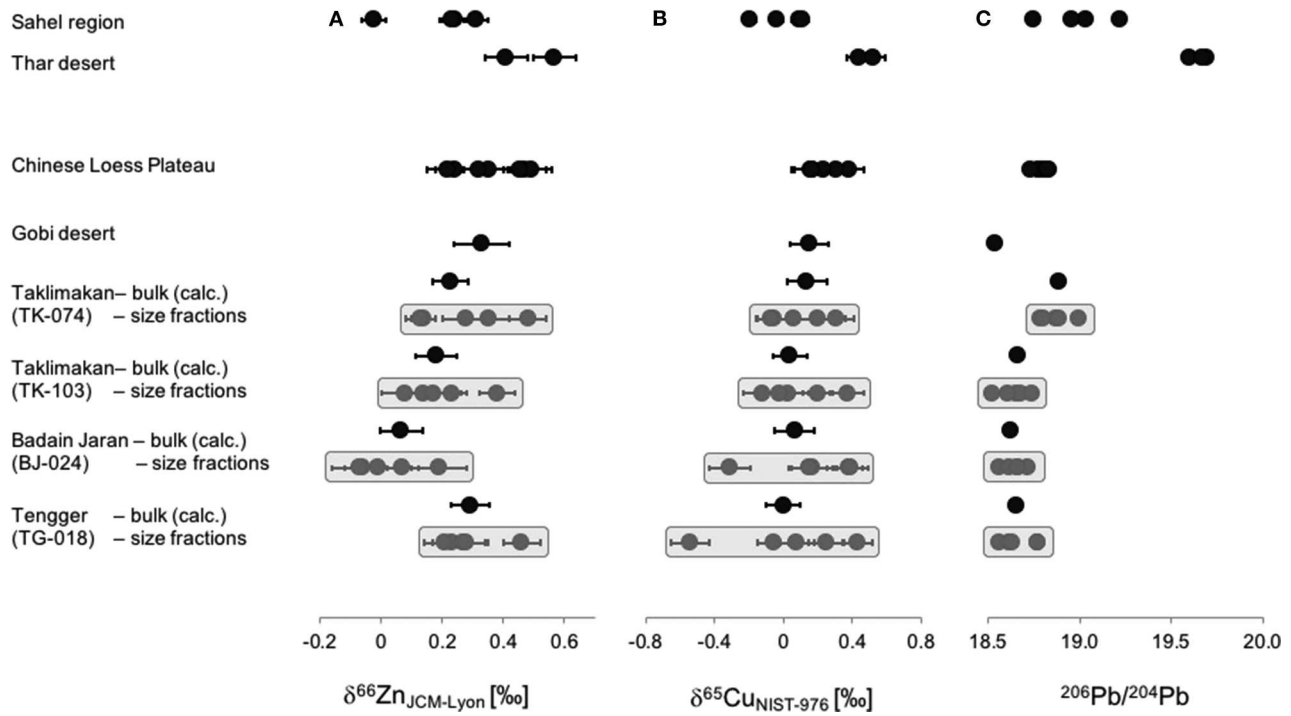

FIGURE 2 | Isotope ratios of Zn (**A**, expressed as $\delta^{66}Zn_{JMC-Lyon}$), Cu (**B**, expressed as $\delta^{65}Cu_{NIST-976}$), and Pb (**C**, expressed as $^{206}Pb/^{204}Pb$) in the mineral dust samples studied in this work. Samples from the Taklimakan, Tengger and Badain Jaran deserts show the measured isotope ratios of the individual size fractions (gray shadows) as well as of the calculated bulk value. The bulk isotopic composition of the elements was calculated using mass balance, i.e., $\delta X_{bulk} = \Sigma\ \delta X_i \times f_i$ or $^{206}Pb/^{204}Pb = \Sigma\ ^{206}Pb/^{204}Pb_i \times f_i$, where i = size fraction, and f_i = abundance of the fraction i with respect to the bulk.

fraction to 41.5 and 84.1 μg/g in the >63 μm size fraction. Lead concentrations are highest in the smallest fraction (39 μg/g) and lowest in the largest fraction (12 μg/g).

Previous studies showed significant variations in the radiogenic isotope compositions of Sr, Nd, and Pb between size fractions of natural mineral dust (Feng et al., 2009). Similarly, we find significant variations in the stable Cu and Zn isotope compositions of the different size fractions compared to analytical precision (**Figure 3**, **Table 3**). For Zn, these variations are up to 0.35‰, for Cu up to 0.97‰. For $^{206}Pb/^{204}Pb$ we observe variations up to 0.22. The larger variability found in Cu compared to Zn is in agreement with the greater variability found for the isotopic composition of Cu in rocks and minerals in general, likely partly controlled by the variable redox states of Cu in nature (Markl et al., 2006). The isotopic composition vs. particle size fraction plots (**Figure 3**), excluding the $\delta^{65}Cu$ values of two samples (TK-074 and BJ-024, discussed below), are similar for Cu and Zn, i.e., a U-shaped curve with the most positive values predominantly in the smallest and largest particle size fractions and more negative values in the mid particle size fractions (**Figure 3**).

The $\delta^{65}Cu_{NIST-976}$ values of the samples from the Tengger desert (TG-018) and the Badain Jaran desert (BJ-024) decrease from the <4 μm to the 4–16 μm size fraction, then increase from −0.54 ± 0.11‰ to +0.43 ± 0.09‰ (TG-018) and −0.31 ± 0.12‰ to +0.39 ± 0.10‰ (BJ-024) in the size fraction >63 μm. The $\delta^{65}Cu_{NIST-976}$ value of the fraction <4 μm and 4–16 μm fractions vary following the pattern of samples TK-074 and TK-103, however, increases in the largest size fractions of sample TK-074 and decreases in the largest size fractions of sample TK-103. The Tengger samples display the largest difference between the size fractions ($\Delta^{65}Cu_{max-min} = 0.97‰$).

The $\delta^{66}Zn_{JMC-Lyon}$ values show a similar pattern for all the four samples analyzed with decreases from the <4 μm to the 16–32 μm fractions and increases from the 16–32 μm to the >63 μm fractions. The Badain Jaran samples encompass the lightest isotopic compositions in all size fractions with minimum $\delta^{66}Zn_{JMC-Lyon}$ values of −0.06 ± 0.06‰ in the 16–32 μm size fraction and −0.07 ± 0.09‰ in the 32–64 μm size fraction. The two Taklimakan samples display the largest differences between the size fractions ($\Delta^{66}Zn_{max-min} = 0.35‰$ for TK-103).

For all four samples, most radiogenic Pb is present in the mid particle size fraction (16–32 μm). Sample TK-103 from the Taklimakan desert had more radiogenic Pb compared to the other samples. The differences between all size fractions is quite similar for all samples with $\Delta^{206}Pb/^{204}Pb_{max-min} \approx 0.2$, and only slightly lower for the Badain Jaran sample ($\Delta^{206}Pb/^{204}Pb_{max-min} \approx 0.16$).

Mineralogical Composition

The mineral compositions were determined in selected bulk samples from the Gobi Desert (MG-09022), the Chinese Loess

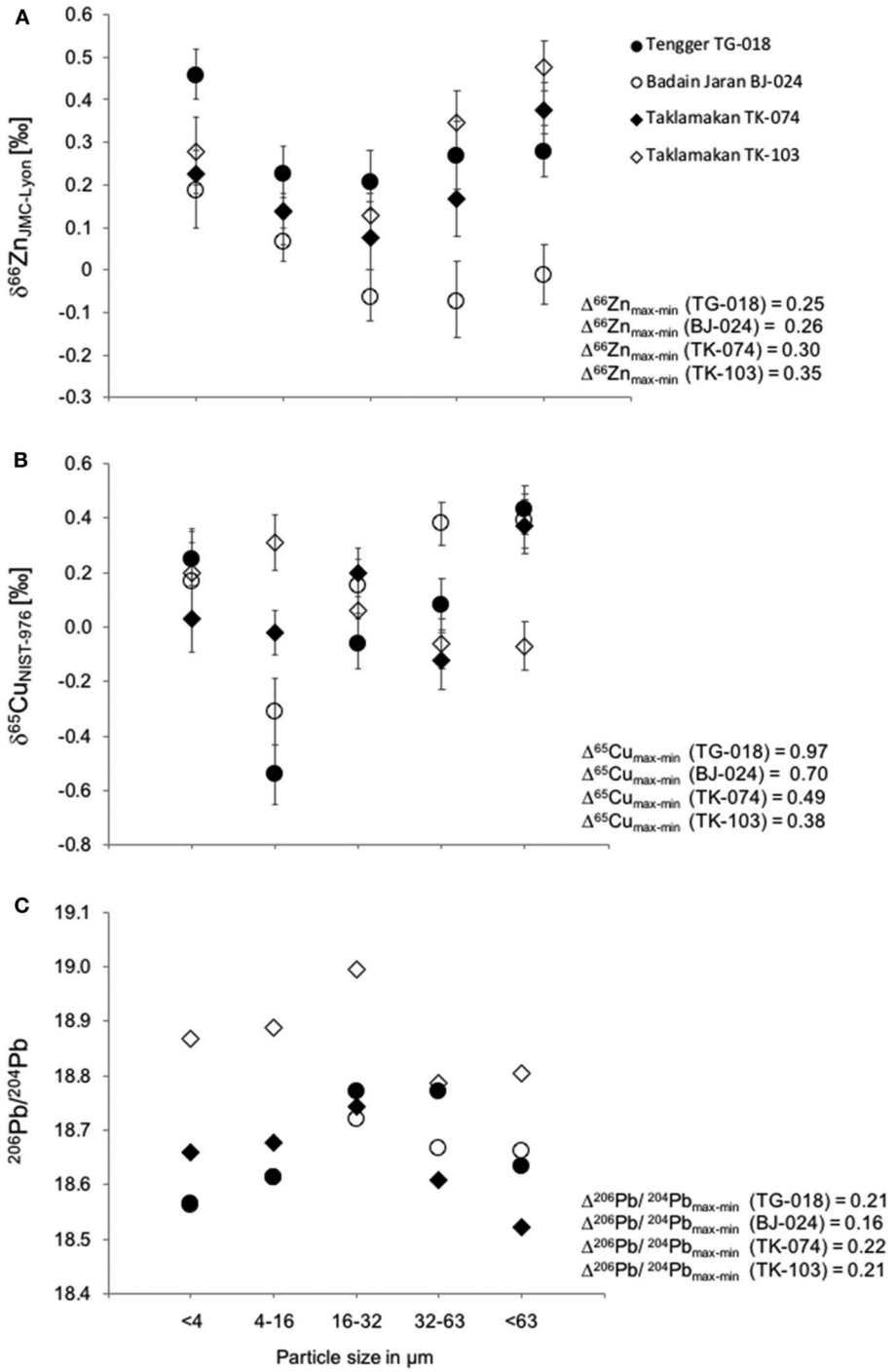

FIGURE 3 | Isotope ratios of Zn **(A)**, Cu **(B)**, and Pb **(C)** in the five different size fractions analyzed in four individual samples from the Tengger desert (TG-018, closed circle), Badain Jaran desert (BJ-024 open circle), and Taklimakan deserts (TK-074, closed diamond and TK-103, open diamond). Also shown are the maximum differences between highest and lowest values for each element and sample (Δ). The error bars for Pb are within the symbol size. Copper and Zn isotope data of TK-074 and TK-103 were published previously as a part of the validation process for our improved analytical procedure (Dong et al., 2013).

Plateau (CLS-20 to−90) and the Thar desert (TDSD-02 and−03) and in different particle size fractions from samples from the Chinese deserts (TG-018, BJ-024, TK-074, TK-103, JY-1) to test the connection between isotopic variability and mineral phases (see also **Table S2**).

All mineral dust samples contain quartz (SiO_2), smectite [$(Ca,Na)_{0.3}(Al,Mg,Fe)_2(Si,Al)_4O_{10}(OH)_2{\cdot}n(H_2O)$], muscovite ($KAl_2(AlSi_3O_{10})(F,OH)_2$), calcite ($CaCO_3$), chlorite [$(Mg,Fe)_3(Si,Al)_4O_{10}(OH)_2$ $(Mg,Fe)_3(OH)_6$], and albite ($NaAlSi_3O_8$). The major mineral phases in the samples from the Chinese

TABLE 4 | Statistical assessment of the relationships between mineralogy, element concentrations and isotope ratios.

	[Zn]	[Cu]	[Pb]	[Sc]	$\delta^{66}Zn_{JMC-Lyon}$	$\delta^{65}Cu_{NIST-976}$	$^{206}Pb/^{204}Pb$	Quartz	Smectite	Albite	Muscovite	Chlorite	Calcite
[Zn]	–	0.56	0.81	0.66	−0.23	−0.24	0.28	−0.78	0.59	−0.40	0.65	0.36	0.25
[Cu]	0.56	–	0.68	0.84	0.03	−0.07	0.32	−0.84	0.77	−0.30	0.46	0.28	0.05
[Pb]	0.81	0.68	–	0.88	0.02	−0.01	0.43	−0.70	0.52	−0.58	0.77	0.13	0.21
[Sc]	0.66	0.84	0.88	–	0.02	−0.06	0.46	−0.84	0.78	−0.48	0.61	0.11	0.25
$\delta^{66}Zn_{JMC-Lyon}$	−0.23	0.03	0.02	0.02	–	0.12	0.23	0.31	−0.26	0.04	−0.04	−0.25	−0.23
$\delta^{65}Cu_{NIST-976}$	−0.24	−0.07	−0.01	−0.06	0.12	–	0.06	0.14	−0.12	−0.42	0.17	−0.44	−0.11
$^{206}Pb/^{204}Pb$	0.28	0.32	0.43	0.46	0.23	0.06	–	0.68	−0.65	0.16	−0.28	−0.29	−0.29
Quartz	−0.78	−0.84	−0.70	−0.84	0.31	0.14	0.68	–	−0.89	0.65	−0.65	−0.02	−0.34
Smectite	0.59	0.77	0.52	0.78	−0.26	−0.12	−0.65	−0.89	–	−0.44	0.39	−0.06	0.06
Albite	−0.40	−0.30	−0.58	−0.48	0.04	−0.42	0.16	0.65	−0.44	–	−0.79	0.31	−0.58
Muscovite	0.65	0.46	0.77	0.61	−0.04	0.17	−0.28	−0.65	0.39	−0.79	–	0.05	0.34
Chlorite	0.36	0.28	0.13	0.11	−0.25	−0.44	−0.29	−0.02	−0.06	0.31	0.05	–	−0.32
Calcite	0.25	0.05	0.21	0.25	−0.23	−0.11	−0.29	−0.34	0.06	−0.58	0.34	−0.32	–

Values represent the Pearson product-moment correlation coefficient, r.

Loess Plateau are smectite (31–50 wt.%), quartz (14–20 wt.%), calcite (9–22 wt.%), and muscovite (6–13 wt.%). Approximately 30 wt.% of quartz, ∼20 wt.% of smectite, and ∼10 wt.% each of calcite, muscovite, and albite are present in both mineral dust samples from the Thar desert. Three wt. % of actinolite ($Ca_2(Mg_{4.5-2.5}Fe^{2+}_{0.5-2.5})Si_8O_{22}(OH)_2$) is present in two samples (CLS-25 and CLS-27) and 8 wt.% of dolomite ($CaMg(CO_3)_2$) in one sample (CLS-20) in the Chinese Loess Plateau. The <4 μm size fraction of the samples from the Chinese deserts contains mainly smectite (51–55 wt.%), muscovite (13–22 wt.%), calcite (8–21 wt.%), and chlorite (5–11 wt.%), and <6 wt.% of quartz and 5 wt.% of albite. The sample from the Gobi desert has similar mineral compositions to the Chinese Loess Plateau dust samples. The mineralogical variations within the size fractions (<4, 4–16, 16–32, 32–63, and >63 μm) were assessed for one bulk sample from the Taklimakan desert (TK-103). We find the quartz phase increases from 5 to 31 wt.%, the albite phase increased from 5 to 21 wt.%, and smectite decreases from 55 to 18 wt.% between the size fractions <4 and >63 μm. Chlorite (8–15 wt.%), calcite (8–13 wt.%), and muscovite (6–16 wt.%) phases are similar among the five size fractions. Dolomite was not identified in any of the <4 μm size fraction samples, but 2–4 wt.% of dolomite was found in the remaining size fractions.

The correlation between isotopic composition, concentrations and mineralogy was assessed using multivariate regression of the entire data set available ($n = 17$). **Table 4** shows the results for the Pearson product-moment correlation coefficient, r; which varies from 1 (perfect positive correlation) to 0 (no correlation) to −1 (perfect negative correlation).

DISCUSSION

The discussion section is organized the following way: First, we discuss the range of Zn and Cu isotope compositions in natural reservoirs compiled from new and published data (**Table S3**). Mineral dust is an important natural aerosol source since several billion tons of soil-derived dust is aerosolized each year, including seasonal pulses from Africa and Asia (Kellogg and Griffin, 2006). Second, we complile and discuss isotopic compositions of potential aerosol source materials derived from anthropogenic activity reported in the literature (**Table S3**). Anthropogenic Zn and Cu sources are important since anthropogenic atmospheric emissions have surpassed natural ones (Rauch and Pacyna, 2009) and anthropogenic sources are manifold, especially in urban areas. Third, we compile $\delta^{66}Zn_{JMC-Lyon}$ and $\delta^{65}Cu_{NIST-976}$ isotope values of urban aerosols from literature and add new data from two Chinese cities. We compare the isotopic composition of aerosols from different cities and discuss the possible influence of the major natural and anthropogenic reservoirs.

Zinc and Cu Isotope Signatures in Mineral Dust and Other Natural Reservoirs

We observe important geographical variations in the isotopic composition of mineral dust (**Figure 2**). The samples from the Thar desert display the heaviest Zn and Cu isotope compositions with $\delta^{66}Zn_{JMC-Lyon} = +0.49 \pm 0.11‰$ and $\delta^{65}Cu_{NIST-976} = +0.48 \pm 0.06‰$ ($n = 2$). In contrast, the samples from the Sahel region and the Badain Jaran desert exhibit the lightest Zn isotope compositions ($\delta^{66}Zn_{JMC-Lyon} = +0.19 \pm 0.15‰$ ($n = 3$), $\delta^{66}Zn_{JMC-Lyon} = +0.07‰$ ($n = 1$), respectively). The mineral dust samples of the Chinese Loess Plateau are heavier with respect to their Zn and Cu isotope compositions than those of Chinese deserts. While the isotopic variability of the different size fractions results in a significant spread (**Figure 2**, Taklimakan, Tengger, and Badain Jaran), the bulk values of the samples collected from each geographical region remain within a small range of $\Delta^{66}Zn_{max-min} = 0.23‰$ and $\Delta^{65}Cu_{max-min} = 0.14‰$, as shown in **Figure 2**. The $^{206}Pb/^{204}Pb$ values for the Chinese deserts and the Loess Plateau fit well in the range of $^{206}Pb/^{204}Pb$ values of 18.648–18.786 derived from a peat bog and proposed to serve as "Asian natural background" by Ferrat et al. (2012b).

Calculated enrichment factors for Zn and Cu are below five for all samples (see **Table 3**), and, thus, we suggest that deposition of

metals from anthropogenic emissions from long range transport in these regions are negligible. There are slight differences between the dust source regions: Chinese dust samples show slightly higher EFs with average values of 2.2 and 1.3 for Cu and Zn, respectively, in the Chinese deserts, and 1.2 and 1.1 for the Chinese Loess Plateau. Both, the Sahel region (average of 0.7 and 0.9 for Zn and Cu, respectively) and the Thar desert (average of 0.5 and 0.4 for Zn and Cu, respectively) have EFs below 1 and, thus again, no anthropogenic influence is assumed.

Figure 4 shows bivariate plots for the isotope ratios of the three elements (Zn, Cu, and Pb) measured. The Zn vs. Pb and Cu vs. Pb plots separate the samples from the Thar desert well. The samples from the Sahel region, from the Chinese desert and the Chinese Loess Plateau tend to be clustered together, while those from the Thar desert plot toward the more radiogenic Pb.

We do not find a clear mineralogical control on the Zn and Cu isotope compositions of mineral dust. A link between the enrichment of light isotopes and clay minerals was observed for Cu and Zn in altered and unaltered hydrothermal deposits (Markl et al., 2006) and in soils (Bigalke et al., 2010). However, we observe similar Zn and Cu signatures for samples with dominant or lesser contributions of clay minerals, such as the samples from the Chinese deserts and the Thar desert. Overall, the multivariate regression analysis of our limited data set suggests no significant associations between mineralogy and Zn or Cu isotope composition (**Tables 4** and **S2**). By contrast, Pb isotope compositions seem interrelated with quartz and smectite abundance, suggesting a possible link between the mineralogy and radiogenic isotope composition of mineral dust.

We observe significant isotope variations between the different size fractions of mineral dust as described in section Concentration and isotope ratios of Cu, Zn, and Pb in particle size fractions. Most samples (except $\delta^{65}Cu_{NIST-976}$ values of TK-074 and BJ-024) display a *U*-shaped curve (**Figure 3**) with the highest δ-values in the smallest and largest particle size fractions and lower values in the mid particle size fractions. The different size fractions for Taklimakan reveal systematic changes for quartz (i.e., an increase from the fine to the coarse fraction) and clay minerals (i.e., a decrease from the fine to the coarse fraction) but not for the other fractions.

Enrichment factors for all mineral dust samples are low (<5) and we do not assume an influence from anthropogenic sources. However, we caution that any minor anthropogenic influence may disproportionately impact the smaller size fractions, due to the potential for long-range transport of fine particles. Both Taklimakan samples show the highest EFs for the smallest size fraction (<4 μm), lower for the medium size fraction (16–32 μm), and smallest for the largest size fraction (>64 μm).

The differences in isotopic ratios between size fractions may have important implications for source apportionment studies as long-range transport of small particles may cause shifts in the isotope signatures of dust in the atmosphere. Mori et al. (2003) showed that the particle sizes changed during long-range transport from China to Japan but that the chemical composition of crustal elements remained nearly constant. But if Cu and Zn isotope compositions vary between different size fractions of the source material, as our new data suggests, then we can expect changes in the isotopic composition along a transect from the source to the sink due to particle size (in addition to fractionation processes during atmospheric transport).

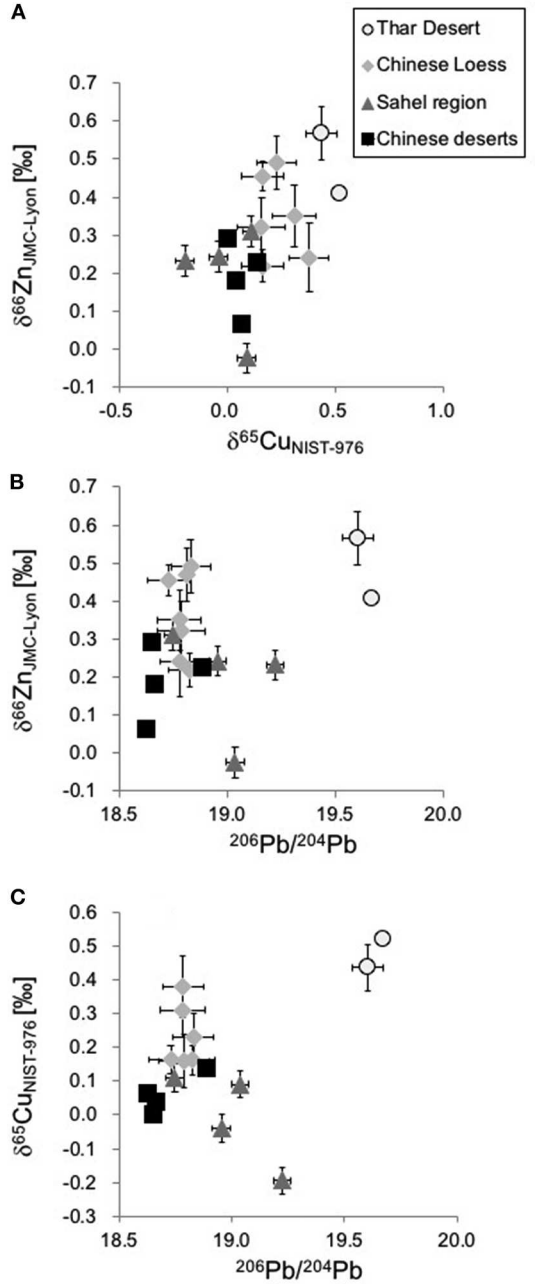

FIGURE 4 | Bivariate plots of the three isotope systems ($\delta^{66}Zn_{JMC-Lyon}$, $\delta^{65}Cu_{NIST-976}$, and $^{206}Pb/^{204}Pb$) in bulk samples. **(A)** $\delta^{66}Zn_{JMC-Lyon}$ vs. $\delta^{65}Cu_{NIST-976}$; **(B)** $\delta^{66}Zn_{JMC-Lyon}$ vs. $^{206}Pb/^{204}Pb$; and **(C)** $\delta^{65}Cu_{NIST-976}$ vs. $^{206}Pb/^{204}Pb$.

In this review we compiled data likely relevant as aerosol sources. A broader review including extra-terrestrial samples and the oceanic reservoirs has recently been presented by Moynier et al. (2017). **Figure 5** comprises the Zn (left panel) and Cu (right panel) isotope ratios of these relevant natural reservoirs, mainly different rock types, as well as unpolluted soils and mineral dust (see also **Table S3**).

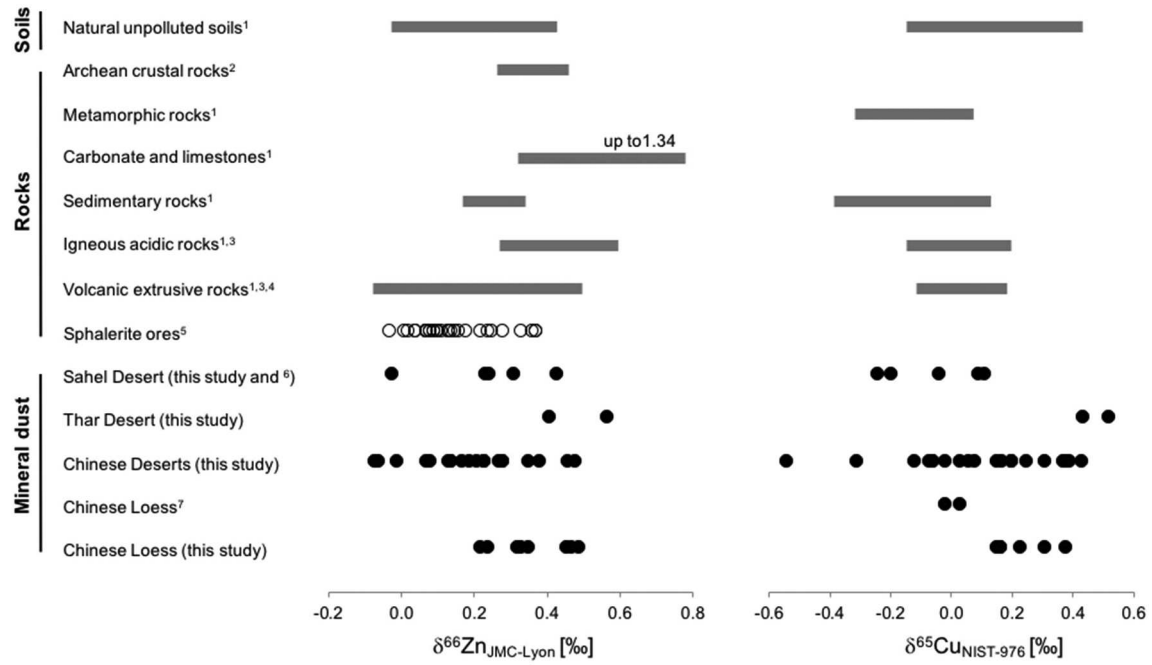

FIGURE 5 | Comparison of measured isotope ratios of Zn (left panel, expressed as $\delta^{66}Zn_{JMC-Lyon}$) and Cu (right panel, expressed as $\delta^{65}Cu_{NIST-976}$) in natural reservoirs (References: 1. Fekiacova et al., 2015; 2. Doucet et al., 2018, 3. Cloquet et al., 2008, 4. Herzog et al., 2009, 5. Sonke et al., 2008, 6. Dong et al., 2013, 7. Li et al., 2009). Note: Mineral dust from this study includes data from different particle size fractions.

$\delta^{66}Zn_{JMC-Lyon}$ is largely positive in igneous rocks, ranging between +0.2 and +0.5‰ in basalts and between +0.4 and +0.6‰ in more acidic rocks, e.g., in granites and granodiorites (Cloquet et al., 2008). The $\delta^{66}Zn_{JMC-Lyon}$ of sphalerite, the major source of Zn concentrates used for industrial purposes (Yin et al., 2016), ranges typically between −0.04 and +0.36‰ (John et al., 2007; Sivry et al., 2008; Sonke et al., 2008; Mondillo et al., 2018). Unpolluted soils and mineral dust span over a similar range of $\delta^{66}Zn_{JMC-Lyon}$ values (**Figure 5**).

For the Cu isotope compositions in natural reservoirs as shown in **Figure 5** (right panel), it is important to note that we include only the products of "primary mineralization." The complete natural range is considerably broader, with products of secondary mineralisation (including products formed during low temperature supergene processes in ore deposits or during metamorphic processes) spanning a considerably broader range of −16 to +10‰ (Mathur et al., 2009; Moynier et al., 2017). Mineral dust $\delta^{65}Cu_{NIST-976}$ values are very similar to those of most common parent rocks and, thus, the Cu isotope composition of mineral dust looks like that of igneous/clastic sedimentary rocks.

Zinc and Cu Isotope Signatures of Anthropogenic Reservoirs

Figure 6 compiles the Cu and Zn isotope compositions of anthropogenic reservoirs. More details can be found in **Table S3**. We divided the anthropogenic reservoirs into non-exhaust traffic derived materials (e.g., brakes and tires; filled circles in **Figure 6**), materials derived from industrial activities (combustion, galvanization, electroplating; open circles in **Figure 6**), and other sources (e.g., contaminated soils, fertilizers, and cement; gray circles in **Figure 6**). To the authors' knowledge, no Cu or Zn isotope compositions of other important aerosol source materials, such as biomass combustion, or train, airplane, and shipping emissions have been studied to date.

For the Zn isotope compositions of anthropogenic reservoirs (**Figure 6**, left panel), we make the following observations:

i) The $\delta^{66}Zn_{JMC-Lyon}$ values including all anthropogenic reservoirs range from −0.73 to +1.49‰. For comparison, $\delta^{66}Zn_{JMC-Lyon}$ values of natural materials compiled in **Figure 5** have a smaller range of −0.07 and +1.34‰, highlighting the broad isotopic range of industrially processed materials. Human activity thus considerably increases the range of Zn isotope ratios for aerosol sources, particularly toward lighter isotopic compositions.

ii) Several anthropogenic materials (tires and brakes, industrial raw materials, health products and cement) plot in the same range as sphalerite (see gray range in **Figure 6**), which is the mineral mainly used to produce concentrates (Yin et al., 2016) that are used in subsequent industrial processes. This similarity would suggest that no significant isotopic fractionation occurs during production of the concentrates or final materials.

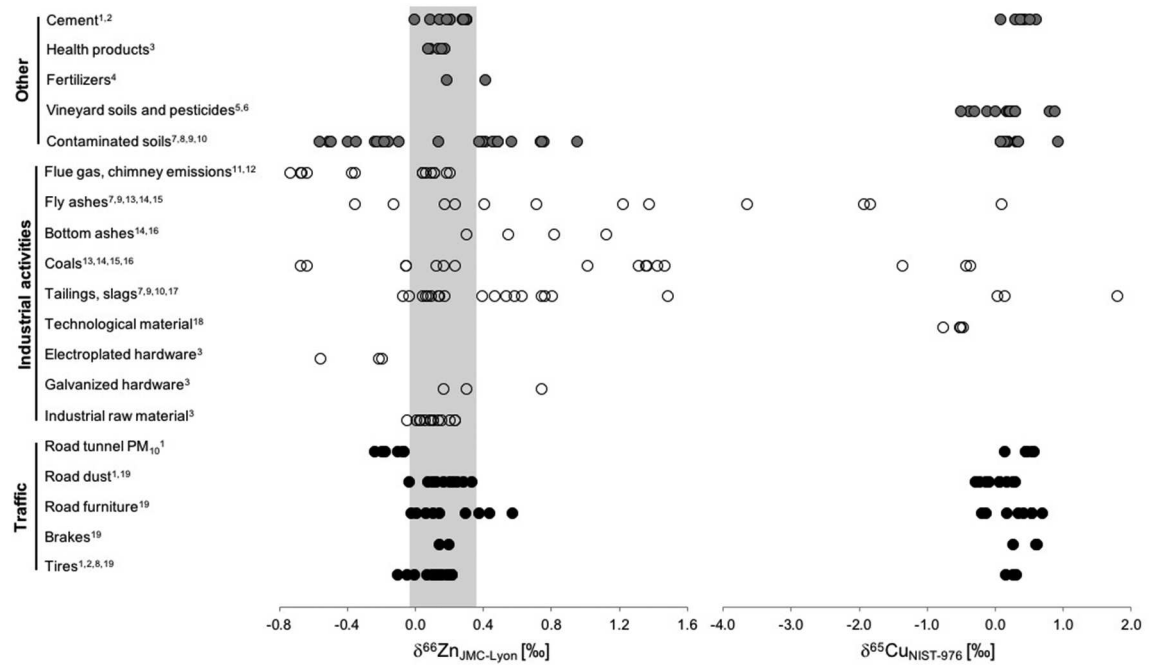

FIGURE 6 | Comparison of measured isotope ratios of Zn (left panel, expressed as $\delta^{66}Zn_{JMC-Lyon}$) and Cu (right panel, expressed as $\delta^{65}Cu_{NIST-976}$) in anthropogenic reservoirs (traffic: filled circles, industrial processes: open circles, other: gray circles). The gray area gives the range of natural sphalerites proposed by Sonke et al. (2008) (References: 1. Souto-Oliveira et al., 2018, 2. Souto-Oliveira et al., 2019, 3. John et al., 2007, 4. Chen et al., 2008, 5. Petit et al., 2013, 6. Blotevogel et al., 2018, 7. Sivry et al., 2008, 8. Thapalia et al., 2010, 9. Bigalke et al., 2010, 10. Juillot et al., 2011, 11. Cloquet et al., 2006, 12. Mattielli et al., 2009, 13. Novak et al., 2016, 14. Ochoa Gonzalez and Weiss, 2015, 15. Voldrichova et al., 2014, 16. Borrok et al., 2010, 17. Gelly et al., 2019, 18. Mihaljevič et al., 2018, 19. Dong et al., 2017).

iii) Some anthropogenic materials are isotopically lighter or heavier than the sphalerite range. These materials were processed either by high-temperature processes/evaporation such as coal combustion or by electroplating and galvanization, thus most likely products from unidirectional fractionation processes. Pulverized coal and a mixture of coal/pet coke combustion led to significant isotope fractionation between the byproducts [the coal fly ash, with $\delta^{66}Zn_{JMC-Lyon}$ =1.23–1.95‰ ($n = 6$), and the bottom ash, with $\delta^{66}Zn_{JMC-Lyon}$ = 0.55–1.13‰ ($n = 3$)] with respect to the starting materials ($\delta^{66}Zn_{JMC-Lyon}$ = 1.02–1.47‰, $n = 5$) (Ochoa Gonzalez and Weiss, 2015). Electroplating causes large isotope effects due to redox reaction (Kavner et al., 2008). Electroplated materials may constitute isotopically distinct metal sources released to the environment as metal wastes and mobilized via corrosion processes. Kavner et al. (2008) studied Zn isotope fractionation during electroplating in a controlled laboratory experiment. They found that the composition of plated Zn metal is enriched in the light isotope (^{64}Zn) after electrochemical reduction with respect to the Zn^{2+} leftover in solution. Similar observations for electroplating during laboratory experiments were reported by Black et al. (observed fractionations varying from $\Delta^{66/64}Zn_{metal-aqueous} = -1.0$ to −3.9‰; Black et al., 2014). These findings are in line with the isotopically light Zn values ($\delta^{66}Zn_{JMC-Lyon} = -0.32 \pm 0.20$‰, $n = 3$) of electroplated hardware measured by John et al. (2007, **Figure 6**). Galvanized hardware displayed isotopically heavier Zn values ($\delta^{66}Zn_{JMC-Lyon} = +0.41 \pm 0.30$‰, $n = 3$; John et al., 2007, **Figure 6**).

We make the following observations for the Cu isotope compositions of anthropogenic reservoirs (**Figure 6**, right panel):

i) $\delta^{65}Cu_{NIST-976}$ values for anthropogenic reservoirs range from −3.6 to +1.8‰. This range is smaller than the considerably broader natural range of −16 to +10‰ (e.g., Mathur et al., 2009; Moynier et al., 2017) if secondary mineralization (formed during low temperature supergene processes in ore deposits or during metamorphic processes) is included.
ii) In comparison to Zn, human activity seems not increase the range of Cu isotope compositions. Possible reason for this might be the higher variability of Cu isotopic compositions in natural reservoirs.
iii) Traffic-related sources have $\delta^{65}Cu_{NIST-976}$ values ranging from −0.18 to +0.71‰, with a median value of +0.34‰.
iv) Contaminated soils spread over a wide range of Cu isotope compositions. For aerosols, soils can be seen as a source (resuspension) or sink (deposition). Most Zn or Cu isotope studies focussed on soils close to (active or historic) mining, refining and/or smelting sites (**Figure 6**, **Table S3**) or for Cu also in vineyard soils.

Comparison of Zn and Cu Isotope Compositions in Urban Aerosols With Natural and Anthropogenic Reservoirs

Figure 7 shows the δ-values for Zn and Cu in urban aerosols. Studies were conducted in several cities, including Barcelona (Spain, Ochoa Gonzalez et al., 2016), London (UK, Ochoa Gonzalez et al., 2016; Dong et al., 2017), Zaragoza (Martín et al., 2018), and Metz (France, Cloquet et al., 2006). Gioia et al. (2008) as well as Souto-Oliveira et al. (2018, 2019) reported Cu and Zn isotope compositions from São Paulo, Brazil. To the authors' knowledge, our data from Beijing and Xi'an provides the first Zn and Cu isotope data for an Asian city.

For the Zn isotope compositions of urban aerosols (**Figure 7**, left panel), we make the following observations:

i) The Zn isotope compositions of aerosols spread over a wide range from $\delta^{66}Zn_{JMC-Lyon}$ of −1.36 to +0.78‰. This range is considerably broader than the range observed for mineral dust or natural unpolluted soils and is more similar to that of the anthropogenic sources discussed in section Zinc and Cu isotope signatures of anthropogenic reservoirs. Generally, $\delta^{66}Zn$ values in aerosols tend toward isotopically values even lighter than those identified for the anthropogenic sources (section Comparison of Zn and Cu isotope compositions in urban aerosols with natural and anthropogenic reservoirs).

ii) The Zn isotope compositions of aerosols can vary considerably within one city. The highest variability ($\Delta^{66}Zn_{max-min}$ = 1.5‰, $n = 62$) to date was found in São Paulo (Souto-Oliveira et al., 2018), which the authors attribute to highly variable source contributions and frequent changing meteorological conditions. In London, smaller temporal and spatial variation were observed but significant differences in particle sizes were also noted (Ochoa Gonzalez et al., 2016).

iii) The two samples from Beijing and Xi'an in China fit well into the observed ranges from other cities. The $\delta^{66}Zn_{JMC-Lyon}$ value from Beijing of −0.36 ± 0.04‰ is lower than the $\delta^{66}Zn_{JMC-Lyon}$ of 0.02 ± 0.04‰ from Xi'an collected at the same time (summer 2011). Beijing is situated further from the dust sources than Xi'an. The isotopically lighter composition in Beijing would be in line with a stronger influence from anthropogenic activities in this city (more industry in Beijing and a mixed commercial-residential area around the sampling site in Beijing, compared to a residential area in Xi'an).

We make the following observations for Cu isotope compositions of urban aerosols (**Figure 7**, right panel):

i) The $\delta^{65}Cu_{NIST-976}$ values spread over a wide range from −0.01 to +0.97‰. One sample from Barcelona is even isotopically lighter with a $\delta^{65}Cu_{NIST-976}$ value of −0.43‰.

ii) Aerosol Cu isotope composition can vary considerably depending on the season. For example, isotopically heavy Cu were detected during the winter season in coarse particles ($PM_{2.5-80}$) in London ($\delta^{65}Cu_{NIST-976}$ ranging between +0.63 and +0.97‰), along with higher EFs and Cu/Sb ratios (Ochoa Gonzalez et al., 2016). The authors attributed this to increased contribution from fossil fuel combustion.

iii) The lighter $\delta^{65}Cu$ values in urban PM, combined with lower Cu/Sb ratios, can be used for source tracing of brake particles (Ochoa Gonzalez et al., 2016; Dong et al., 2017).

SUMMARY AND CONCLUSIONS

1 Based on our synthesis of new and published data, we propose the following isotopic ranges (and means if statistically reasonable) of Zn and Cu in anthropogenic and natural reservoirs (see **Table S3** and **Figures 5**, **6** for references):

a **Mineral dust derived from:**

i) Sahara Desert (Sahel region):
$\delta^{66}Zn_{JMC-Lyon}$: between 0.0 and +0.4‰ ($n = 5$)
$\delta^{65}Cu_{NIST-976}$: between −0.2 and +0.1‰ ($n = 5$)

ii) Chinese deserts and Loess Plateau:
$\delta^{66}Zn_{JMC-Lyon}$: between −0.1 and +0.5‰, mean value +0.24‰ ($n = 28$)
$\delta^{65}Cu_{NIST-976}$: between −0.5 and +0.4‰, mean value +0.12‰ ($n = 29$)

iii) Thar desert:
$\delta^{66}Zn_{JMC-Lyon}$: between +0.4 and +0.6‰ ($n = 2$)
$\delta^{65}Cu_{NIST-976}$: between +0.4 and +0.5‰ ($n = 2$)

b **Particles derived from non-exhaust traffic emissions:**
$\delta^{66}Zn_{JMC-Lyon}$: between −0.1 and +0.6‰, mean value +0.16‰ ($n = 28$)
$\delta^{65}Cu_{NIST-976}$: between −0.2 and +0.7‰, mean value +0.34‰ ($n = 14$)

c **Particles derived from combustion:**
$\delta^{66}Zn_{JMC-Lyon}$: between −0.73 and +0.21‰, mean value −0.18‰ ($n = 14$)

d **Particles derived from electroplating:**
$\delta^{66}Zn_{JMC-Lyon}$: between −0.55 and −0.19‰ ($n = 3$)

e **Particles derived from galvanization:**
$\delta^{66}Zn_{JMC-Lyon}$: between +0.17 and +0.75‰ ($n = 3$)

2 We present new Cu, Zn, and Pb isotope compositions for mineral dust from major deserts in Asia and Africa and from aerosols collected in Beijing and Xi'an, China.

3 We show that human activities introduce a wide range of Zn isotope compositions into the environment, highlighting that humans are changing the global geochemical cycles of Zn isotopes.

4 We do not find Zn isotope fractionation between sphalerite (natural reservoir) and ore concentrate (anthropogenic reservoir), while significant Zn isotope fractionation does occur through anthropogenic activities. We also suggest that Zn isotope fingerprints are a promising tracer to differentiate between combustion vs. non-combustion sources in aerosols and can play a major contribution to air quality assessments in urban environments.

5 Copper isotopes seem either not fractionate to the same significant extent during combustion and other industrial

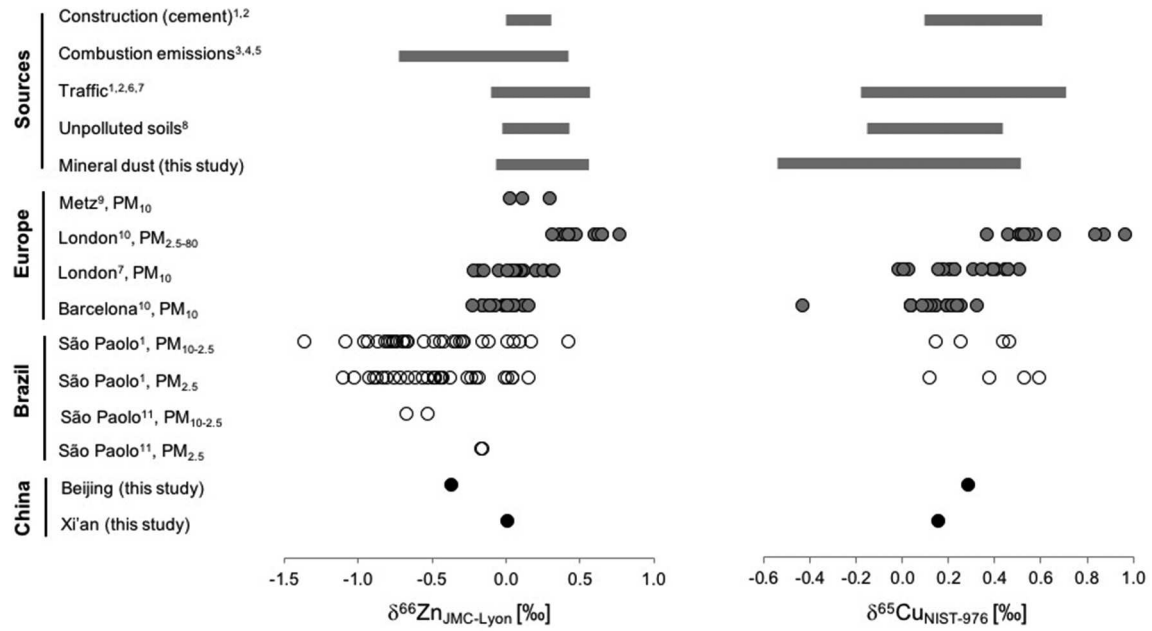

FIGURE 7 | Comparison of measured isotope ratios of Zn (left panel, expressed as $\delta^{66}Zn_{JMC-Lyon}$) and Cu (right panel, expressed as $\delta^{65}Cu_{NIST-976}$) in urban aerosols from Europe (gray circles), Brazil (open circles), and China (filled circles). Additionally, ranges of the most important aerosol sources are given. (References: 1. Souto-Oliveira et al., 2018, 2. Souto-Oliveira et al., 2019, 3. Mattielli et al., 2009, 4. Shiel et al., 2010, 5. Gelly et al., 2019, 6. Thapalia et al., 2010, 7. Dong et al., 2017, 8. Fekiacova et al., 2015, 9. Cloquet et al., 2006, 10. Ochoa Gonzalez et al., 2016, 11. Gioia et al., 2008).

processes or could reflect the wide isotope range of natural reservoirs.

DATA AVAILABILITY STATEMENT

All datasets generated for this study are included in the article/**Supplementary Material**.

AUTHOR CONTRIBUTIONS

NS led analysis and compilation of data and wrote the paper and made all the figures. The paper manuscript was subsequently revised by all authors, each of whom contributed to the intellectual content. SD performed most of the laboratory work, including concentration and isotope analysis of the new samples presented in this paper. YS provided all mineral dust and aerosol samples from China including the size fractionated samples. JN performed XRD analyses and led the interpretation of the mineralogical data.

ACKNOWLEDGMENTS

We thank Barry Coles, Tim Arnold, and Catherine Unsworth for assistance in the laboratory and two reviewers and the editor for their helpful suggestions on a previous version of this manuscript. We thank Paola Formenti and Earl Williams for collecting soil dust samples from Mali. We acknowledge financial support from the UK–China Scholarships for Excellence for SD and from the German Research Foundation (DFG) for NS (SCHL 1908/2-1). SL acknowledges support from a NERC independent research fellowship (NE/P018181/1). RO thanks The European Commission (FP7-PEOPLE-2012-IEF) for funding the project ISOTRACE (proposal 329878).

SUPPLEMENTARY MATERIAL

The Supplementary Material for this article can be found online at: https://www.frontiersin.org/articles/10.3389/feart.2020.00167/full#supplementary-material

REFERENCES

Adamson, I. Y. R., Prieditis, H., Hedgecock, C., and Vincent, R. (2000). Zinc is the toxic factor in the lung response to an atmospheric particulate sample. *Toxicol. Appl. Pharm.* 166, 111–119. doi: 10.1006/taap.2000.8955

Aebischer, S., Cloquet, C., Carignan, J., Maurice, C., and Pienitz, R. (2015). Disruption of the geochemical metal cycle during mining: multiple isotope studies of lake sediments from Schefferville, subarctic Québec. *Chem. Geol.* 412, 167–178. doi: 10.1016/j.chemgeo.2015.07.028

Aranda, S., Borrok, D. M., Wanty, R. B., and Balistrieri, L. S. (2012). Zinc isotope investigation of surface and pore waters in a mountain watershed impacted by acid rock drainage. *Sci. Total Environ.* 420, 202–213. doi: 10.1016/j.scitotenv.2012.01.015

Araújo, D. F., Boaventura, G. R., Viers, J., Mulholland, D. S., Weiss, D., Araújo, D., et al. (2016). Ion exchange chromatography and mass bias

correction for accurate and precise Zn isotope ratio measurements in environmental reference materials by MC-ICP-MS. *J. Braz. Chem. Soc*. 1–11. doi: 10.5935/0103-5053.20160167

Araújo, D. F., Machado, W., Weiss, D., Mulholland, D. S., Garnier, J., Souto-Oliveira, C. E., et al. (2018). Zinc isotopes as tracers of anthropogenic sources and biogeochemical processes in contaminated mangroves. *Appl. Geochem*. 95, 25–32. doi: 10.1016/j.apgeochem.2018.05.008

Archer, C., Andersen, M. B., Cloquet, C., Conway, T. M., Dong, S., Ellwood, M., et al. (2017). Inter-calibration of a proposed new primary reference standard AA-ETH Zn for zinc isotopic analysis. *J. Anal. At. Spectrom*. 32, 415–419. doi: 10.1039/C6JA00282J

Arnold, T., Schonbachler, M., Rehkamper, M., Dong, S., Zhao, F. J., Kirk, G. J., et al. (2010). Measurement of zinc stable isotope ratios in biogeochemical matrices by double-spike MC-ICPMS and determination of the isotope ratio pool available for plants from soil. *Anal. Bioanal. Chem*. 398, 3115–3125. doi: 10.1007/s00216-010-4231-5

Bigalke, M., Weyer, S., Kobza, J., and Wilcke, W. (2010). Stable Cu and Zn isotope ratios as tracers of sources and transport of Cu and Zn in contaminated soil. *Geochim. Cosmochim. Acta* 74, 6801–6813. doi: 10.1016/j.gca.2010.08.044

Black, J. R., John, S. G., and Kavner, A. (2014). Coupled effects of temperature and mass transport on the isotope fractionation of zinc during electroplating. *Geochim. Cosmochim. Acta* 124, 272–282. doi: 10.1016/j.gca.2013.09.016

Blotevogel, S., Oliva, P., Sobanska, S., Viers, J., Vezin, H., Audry, S., et al. (2018). The fate of Cu pesticides in vineyard soils: a case study using δ65Cu isotope ratios and EPR analysis. *Chem. Geol*. 477, 35–46. doi: 10.1016/j.chemgeo.2017.11.032

Borrok, D. M., Gier,é, R., Ren, M., and Landa, E. R. (2010). Zinc isotopic composition of particulate matter generated during the combustion of coal and coal and tire-derived fuels. *Environ. Sci. Technol*. 44, 9219–9224. doi: 10.1021/es102439g

Brand, W. A., Coplen, T. B., Vogl, J., Rosner, M., and Prohaska, T. (2014). Assessment of international reference materials for isotope-ratio analysis (IUPAC Technical Report). *Pure Appl. Chem*. 86, 425–467. doi: 10.1515/pac-2013-1023

Brewer, G. J. (2010). Copper toxicity in the general population. *Clin. Neurophysiol*. 121, 459–460. doi: 10.1016/j.clinph.2009.12.015

Calvo, A. I., Alves, C., Castro, A., Pont, V., and Vicente, A. M., Fraile, R. (2013). Research on aerosol sources and chemical composition: past, current and emerging issues. *Atmos. Res*. 120–121, 1–28. doi: 10.1016/j.atmosres.2012.09.021

Chen, J., Gaillardet, J., and Louvat, P. (2008). Zinc isotopes in the Seine River waters, France: a probe of anthropogenic contamination. *Environ. Sci. Technol*. 42, 6494–6501. doi: 10.1021/es800725z

Chen, Y., Schleicher, N., Cen, K., Liu, X., Yu, Y., Zibat, V., et al. (2016). Evaluation of impact factors on PM2.5 based on long-term chemical components analyses in the megacity Beijing, China. *Chemosphere* 155, 234–242. doi: 10.1016/j.chemosphere.2016.04.052

Cloquet, C., Carignan, J., Lehmann, M. F., and Vanhaecke, F. (2008). Variations in the isotopic composition of zinc in the natural environment and the use of zinc isotopes in biogeosciences: a review. *Anal. Bioanal. Chem*. 390, 451–463. doi: 10.1007/s00216-007-1635-y

Cloquet, C., Carignan, J., and Libourel, G. (2006). Isotopic composition of Zn and Pb atmospheric depositions in an urban/peri-urban area of Northeastern France. *Environ. Sci. Technol*. 40, 6552–6600. doi: 10.1021/es0609654

Colbeck, I., and Lazaridis, M. (2010). Aerosols and environmental pollution. *Naturwissenschaften* 97, 117–131. doi: 10.1007/s00114-009-0594-x

Cressey, G., and Schofield, P. F. (1996). Rapid whole-pattern profile-stripping method for the quantification of multiphase samples. *Powder Diffr*. 11, 35–39. doi: 10.1017/S0885715600008885

Debret, B., Beunon, H., Mattielli, N., Andreani, M., Ribeiro da Costa, I., and Escartin, J. (2018). Ore component mobility, transport and mineralization at mid-oceanic ridges: a stable isotopes (Zn, Cu, and Fe) study of the Rainbow massif (Mid-Atlantic Ridge 36?14'N). *Earth Planet. Sci. Lett* 503, 170–180. doi: 10.1016/j.epsl.2018.09.009

Deng, T.-H.-B., Cloquet, C., Tang, Y.-T., Sterckeman, T., Echevarria, G., Estrade, N., et al. (2014). Nickel and Zinc isotope fractionation in hyperaccumulating and nonaccumulating plants. *Environ. Sci. Technol*. 48, 11926–11933. doi: 10.1021/es5020955

Dinis, L., Gammon, P., Savard, M. M., Bégin, C., Girard, I., J., et al. (2018). Puzzling Zn isotopes in spruce tree-ring series. *Chem. Geol*. 476, 171–179. doi: 10.1016/j.chemgeo.2017.11.015

Dolgopolova, A., Weiss, D. J., Seltmann, R., Kober, B., Mason, T. F. D., Coles, B., et al. (2006). Use of isotope ratios to assess sources of Pb and Zn dispersed in the environment during mining and ore processing within the Orlovka-Spokoinoe mining site (Russia). *Appl. Geochem*. 21, 563–579. doi: 10.1016/j.apgeochem.2005.12.014

Dong, S., Ochoa Gonzalez, R., Harrison, R. M., Green, D., North, R., Fowler, G., et al. (2017). Isotopic signatures suggest important contributions from recycled gasoline, road dust and non-exhaust traffic sources for copper, zinc and lead in PM10 in London, United Kingdom. *Atmos. Environ*. 165, 88–98. doi: 10.1016/j.atmosenv.2017.06.020

Dong, S., Weiss, D. J., Strekopytov, S., Kreissig, K., Sun, Y., Baker, A. R., et al. (2013). Stable isotope ratio measurements of Cu and Zn in mineral dust (bulk and size fractions) from the Taklimakan Desert and the Sahel and in aerosols from the eastern tropical North Atlantic Ocean. *Talanta* 114, 103–109. doi: 10.1016/j.talanta.2013.03.062

Doucet, L. S., Laurent, O., Mattielli, N., and Debouge, W. (2018). Zn isotope heterogeneity in the continental lithosphere: new evidence from Archean granitoids of the northern Kaapvaal craton, South Africa. *Chem. Geol*. 476, 260–271. doi: 10.1016/j.chemgeo.2017.11.022

Doucet, L. S., Mattielli, N., Ionov, D. A., Debouge, W., and Golovin, A. V. (2016). Zn isotopic heterogeneity in the mantle: a melting control? *Earth Planet. Sci. Lett*. 451, 232–240. doi: 10.1016/j.epsl.2016.06.040

Duan, J., and Tan, J. (2013). Atmospheric heavy metals and Arsenic in China: situation, sources and control policies. *Atmos. Environ*. 74, 93–101. doi: 10.1016/j.atmosenv.2013.03.031

Ehrlich, S., Butler, I., Halicz, L., Rickard, D., Oldroyd, A., and Matthews, A. (2004). Experimental study of the copper isotope fractionation between aqueous Cu(II) and covellite, CuS. *Chem. Geol*. 209, 259–269. doi: 10.1016/j.chemgeo.2004.06.010

Fekiacova, Z., Cornu, S., and Pichat, S. (2015). Tracing contamination sources in soils with Cu and Zn isotopic ratios. *Sci. Total Environ*. 517, 96–105. doi: 10.1016/j.scitotenv.2015.02.046

Feng, J. L., Zhu, L. P., Zhen, X. L., and Hu, Z. G. (2009). Grain size effect on Sr and Nd isotopic compositions in eolian dust: implications for tracing dust provenance and Nd model age. *Geochem. J*. 43, 123–131. doi: 10.2343/geochemj.1.0007

Ferrat, M., Langmann, B., Cui, Q., and Weiss, D. J. (2013). Numerical simulations of dust transport to the eastern Qinghai-Tibetan Plateau: comparison of model results with a Holocene peat record of dust deposition. *J. Geophys. Res. Atmos*. 118, 4597–4609. doi: 10.1002/jgrd.50275

Ferrat, M., Strekopytov, S., Unsworth, C., Dong, S., Sun, Y., Spiro, B., et al. (2011). Improved provenance tracing of Asian dust sources using rare earth elements and selected trace elements for palaeomonsoon studies on the eastern Tibetan Plateau. *Geochim. Cosmochim. Acta* 75, 6374–6399. doi: 10.1016/j.gca.2011.08.025

Ferrat, M., Weiss, D. J., Dong, S., Spiro, B., Large, D., Sun, Y., et al. (2012a). Natural fluxes and isotopic trends of Pb in atmospheric deposition of Asian dust over the eastern Qinghai-Tibetan Plateau. *Geochim. Cosmochim. Acta* 82, 4–22. doi: 10.1016/j.gca.2010.10.031

Ferrat, M., Weiss, D. J., and Strekopytov, S. (2012b). A single procedure for the accurate and precise quantification of the rare earth elements, Sc, Y, Th and Pb in dust and peat for provenance tracing in climate and environmental studies. *Talanta* 93, 415–423. doi: 10.1016/j.talanta.2012.01.052

Fuzzi, S., Baltensperger, U., Carslaw, K., Decesar, S., Denier van der Gon, H., Facchini, M. C., et al. (2015). Particulate matter, air quality and climate: lessons learned and future needs. *Atmos. Chem. Phys*., 15, 8217–8299. doi: 10.5194/acp-15-8217-2015

Gelly, R., Fekiacova, Z., Guihou, A., Doelsch, E., Deschamps, P., and Keller, C. (2019). Lead, zinc, and copper redistributions in soils along a deposition gradient from emissions of a Pb-Ag smelter decommissioned 100 years ago. *Sci. Total Environ*. 665, 502–512. doi: 10.1016/j.scitotenv.2019.02.092

Gioia, S., Weiss, D. J., Coles, B. J., Arnold, T., and Babinski, M. (2008). Accurate and precise measurements of Zn isotopes in aerosols. *Anal. Chem*. 80, 9776–9780. doi: 10.1021/ac8019587

Guinoiseau, D., Gélabert, A., Moureau, J., Louvat, P., and Benedetti, M. F. (2016). Zn isotope fractionation during sorption onto kaolinite. *Environ. Sci. Technol*. 50, 1844–1852. doi: 10.1021/acs.est.5b05347

Herzog, G. F., Moynier, F., Albarède, F., and Berezhnoy, A. A. (2009). Isotopic and elemental abundances of copper and zinc in lunar samples, Zagami, Pele's hairs, and a terrestrial basalt. *Geochim. Cosmochim. Acta* 73, 5884–5904. doi: 10.1016/j.gca.2009.05.067

John, S. G., Park, J. G., Zhan, Z. T., and Boyle, E. A. (2007). The isotopic composition of some common forms of anthropogenic zinc. *Chem. Geol*. 245, 61–69. doi: 10.1016/j.chemgeo.2007.07.024

Juillot, F., Maréchal, C., Morin, G., Jouvin, D., Cacaly, S., Telouk, P., et al. (2011). Contrasting isotopic signatures between anthropogenic and geogenic Zn and evidence for post-depositional fractionation processes in smelter-impacted soils from Northern France. *Geochim. Cosmochim. Acta* 75, 2295–2308. doi: 10.1016/j.gca.2011.02.004

Kavner, A., John, S. G., Sass, S., and Boyle, E. A. (2008). Redox-driven stable isotope fractionation in transition metals: application to Zn electroplating. *Geochim. Cosmochim. Acta* 72, 1731–1741. doi: 10.1016/j.gca.2008.01.023

Kellogg, C. A., and Griffin, D. W. (2006). Aerobiology and the global transport of desert dust. *Trends Ecol. Evol*. 21, 638–644. doi: 10.1016/j.tree.2006.07.004

Köbberich, M., and Vance, D. (2019). Zn isotope fractionation during uptake into marine phytoplankton: implications for oceanic zinc isotopes. *Chem. Geol*. 523, 154–161. doi: 10.1016/j.chemgeo.2019.04.004

Kříbek, B., Šípková, A., Ettler, V., Mihaljevič, M., Majer, V., Knésl, I., et al. (2018). Variability of the copper isotopic composition in soil and grass affected by mining and smelting in Tsumeb. *Namibia. Chem. Geol*. 493, 121–135. doi: 10.1016/j.chemgeo.2018.05.035

Kusonwiriyawong, C., Bigalke, M., Cornu, S., Montagne, D., Fekiacova, Z., Lazarov, M., et al. (2017). Response of copper concentrations and stable isotope ratios to artificial drainage in a French Retisol. *Geoderma* 300, 44–54. doi: 10.1016/j.geoderma.2017.04.003

Lerman, A., Lal, D., and Dacey, M. F. (1974). "Stokes' settling and chemical reactivity of suspended particles in natural waters," in *Suspended Solids in Water*. ed R. J. Gibbs (New York, NY: Plenum Press), 17–47. doi: 10.1007/978-1-4684-8529-5_2

Li, W., Jackson, S. E., Pearson, N. J., Alard, O., and Chappell, B. W. (2009). The Cu isotopic signature of granites from the Lachlan Fold Belt, SE Australia. *Chem. Geol*. 258, 38–49. doi: 10.1016/j.chemgeo.2008.06.047

Little, S. H., Vance, D., Walker-Brown, C., and Landing, W. M. (2014). The oceaninc mass balance of copper and zinc isotopes, investigated by analysis of their inputs, and outputs to ferrommanganese oxide sediments. *Geochim. Cosmochim. Acta* 125, 673–693. doi: 10.1016/j.gca.2013.07.046

Liu, S.-A., Liu, P.-P., Lv, Y., Wang, Z.-Z., and Dai, J.-G. (2019). Cu and Zn isotope fractionation during oceanic alteration: implications for Oceanic Cu and Zn cycles. *Geochim. Cosmochim. Acta* 257, 191–205. doi: 10.1016/j.gca.2019.04.026

Mahowald, N. M., Baker, A. R., Bergametti, G., Brooks, N., Duce, R. A., Jickells, T. D., et al. (2005). Atmospheric global dust cycle and iron inputs to the ocean. *Global Biogeochem. Cycles* 19, doi: 10.1029/2004GB002402

Maréchal, C. N., Nicolas, E., Douchet, C., and Albarède, F. (2000). Abundance of zinc isotopes as a marine biogeochemical tracer. *Geochem. Geophys. Geosyst*. 1, 1015. doi: 10.1029/1999GC000029

Maréchal, C. N., Télouk, P., and Albarède, F. (1999). Precise analysis of copper and zinc isotopic compositions by plasma-source mass spectrometry. *Chem. Geol*. 156, 251–273. doi: 10.1016/S0009-2541(98)00191-0

Marina-Montes, C., Pérez-Arribas, L. V., Escudero, M., Anzano, J., and Cáceres, J. O. (2020). Heavy metal transport and evolution of atmospheric aerosols in the Antarctic region. *Sci. Total Environ*. 721:137702. doi: 10.1016/j.scitotenv.2020.137702

Markl, G., Lahaye, Y., and Schwinn, G. (2006). Copper isotopes as monitors of redox processes in hydrothermal mineralization. *Geochim. Cosmochim. Acta* 70, 4215–4228. doi: 10.1016/j.gca.2006.06.1369

Martín, A., Caldelas, C., Weiss, D., Aranjuelo, I., and Navarro, E. (2018). Assessment of Metal Immission in Urban Environments Using Elemental Concentrations and Zinc Isotope Signatures in Leaves of Nerium oleander. *Environ. Sci. Technol*. 52, 2071–2080. doi: 10.1021/acs.est.7b00617

Mason, T. F. D., Weiss, D. J., Chapman, J. B., Wilkinson, J. J., Tessalina, S. G., Spiro, B., et al. (2005). Zn and Cu isotopic variability in the Alexandrinka volcanic-hosted massive sulphide (VHMS) ore deposit, Urals, Russia. *Chem. Geol*. 221, 170–187. doi: 10.1016/j.chemgeo.2005.04.011

Mathur, R., Titley, S., Barra, F., Brantley, S., Wilson, M., Phillips, A., et al. (2009). Exploration potential of Cu isotope fractionation in porphyry copper deposits. *J. Geochem. Explor*. 102, 1–6. doi: 10.1016/j.gexplo.2008.09.004

Mattielli, N., Petit, J. C. J., Deboudt, K., Flament, P., Perdrix, E., Taillez, A., et al. (2009). Zn isotope study of atmospheric emissions and dry depositions within a 5 km radius of a Pb-Zn refinery. *Atmos. Environ*. 43, 1265–1272. doi: 10.1016/j.atmosenv.2008.11.030

Mihaljevič, M., Jarošíková, A., Ettler, V., Vaněk, A., PeníŽek, V., Kríbek, B., et al. (2018). Copper isotopic record in soils and tree rings near a copper smelter, Copperbelt, Zambia. *Sci. Total Environ*. 621, 9–17. doi: 10.1016/j.scitotenv.2017.11.114

Moeller, K., Schoenberg, R., Pedersen, R., Weiss, D. J., and Dong, S. (2012). Calibration of the new certified isotopic reference materials ERM-AE647 (Cu) and IRMM-3702 (Zn) against the previously used NIST SRM 976 (Cu) and 'JMC Lyon' (Zn) solutions–a new reference scale for copper and zinc isotope determinations. *Geostand. Geoanal. Res*. 36, 177–199. doi: 10.1111/j.1751-908X.2011.00153.x

Moffet, R. C., de Foy, B., Molina, L. T., Molina, M. J., and Prather, K. A. (2008). Measurement of ambient aerosols in northern Mexico City by single particle mass spectrometry. *Atmos. Chem. Phys*. 8, 4499–4516. doi: 10.5194/acp-8-4499-2008

Mondillo, N., Wilkinson, J. J., Boni, M., Weiss, D. J., and Mathur, R. (2018). A global assessment of Zn isotope fractionation in secondary Zn mineral from sulfide and non-sulfide ore deposits and model for fractionation control. *Chem. Geol*. 500, 182–193. doi: 10.1016/j.chemgeo.2018.09.033

Moore, R. E. T., Larner, F., Coles, B. J., and Rehkämper, M. (2017). High precision Zinc stable isotope measurement of certified biological reference materials using the double spike technique and multiple collector-ICP-MS. *Anal. Bioanal. Chem*. 409, 2941–2950. doi: 10.1007/s00216-017-0240-y

Moreno, T., Querol, X., Alastuey, A., and Gibbons, W. (2009). Identification of chemical tracers in the characterisation and source apportionment of inhalable inorganic airborne particles: an overview. *Biomarkers* 14, 17–22. doi: 10.1080/13547500902965435

Moreno, T., Querol, X., Alastuey, A., Viana, M., Salvador, P., Sánchez de la Campac, A., et al. (2006). Variations in atmospheric PM trace metal content in Spanish towns: illustrating the chemical complexity of the inorganic urban aerosol cocktail. *Atmos. Environ*. 40, 6791–6803. doi: 10.1016/j.atmosenv.2006.05.074

Mori, I., Nishikawa, M., Tanimura, T., and Quan, H. (2003). Change in size distribution and chemical composition of kosa (Asian dust) aerosol during long-range transport. *Atmos. Environ*. 37, 4253–4263. doi: 10.1016/S1352-2310(03)00535-1

Moynier, F., Vance, D., Fujii, T., and Savage, P. (2017). The isotope geochemistry of Zinc and Copper. *Rev. Mineral. Geochem* 82, 543–600. doi: 10.2138/rmg.2017.82.13

Nelson, J., Wasylenki, L., Bargar, J. R., and Brown, J.r,., G. E., Maher, K. (2017). Effects of surface structural disorder and surface coverage on isotopic fractionation during Zn(II) adsorption onto quartz and amorphous silica surfaces. *Geochim. Cosmochim. Acta* 215, 354–376. doi: 10.1016/j.gca.2017.08.003

Novak, M., Sipkova, A., Chrastny, V., Stepanova, M., Voldrichova, P., Veselovsky, F., et al. (2016). Cu-Zn isotope constraints on the provenance of air pollution in Central Europe: using soluble and insoluble particles in snow and rime. *Environ. Pollution* 218, 1135–1146. doi: 10.1016/j.envpol.2016.08.067

Ochoa Gonzalez, R., Strekopytov, S., Amato, F., Querol, X., Reche, C., and Weiss, D. (2016). New insights from zinc and copper isotopic compositions

into the sources of atmospheric particulate matter from two major European Cities. *Environ. Sci. Technol.* 50, 9816–9824. doi: 10.1021/acs.est.6b00863

Ochoa Gonzalez, R., and Weiss, D. (2015). Zinc isotope variability in three coal-fired power plants: a predictive model for determining isotopic fractionation during combustion. *Environ. Sci. Technol.* 49, 12560–12567. doi: 10.1021/acs.est.5b02402

Peel, K., Weiss, D. J., and Sigg, L. (2009). Zinc isotope composition of settling particles as a proxy for biogeochemical processes in lakes: insights from the eutrophic Lake Greifen, Switzerland. *Limnol. Oceanogr.* 54, 1699–1708. doi: 10.4319/lo.2009.54.5.1699

Peréz Rodríguez, N., Engström, E., Rodushkin, I., Nason, P., and Alakangas, L., Öhlander, B. (2013). Copper and iron isotope fractionation in mine tailings at the Laver and Kristineberg mines, northern Sweden. *Appl. Geochem.* 32, 204–215. doi: 10.1016/j.apgeochem.2012.10.012

Petit, J. C. J., de Jong, J., Chou, L., Mattielli, N. (2008). Development of Cu and Zn isotope MC-ICP-MS measurements: application to suspended particulate matter and sediments from the Scheldt Estuary. *Geostand. Geoanal. Res.* 32, 149–166. doi: 10.1111/j.1751-908X.2008.00867.x

Petit, J. C. J., Schäfer, J., Coynel, A., Blanc, G., Deycard, V. N., Derriennic, H., et al. (2013). Anthropogenic sources and biogeochemical reactivity of particulate and dissolved Cu isotopes in the turbidity gradient of the Garonne River (France). *Chem. Geol.* 359, 125–135. doi: 10.1016/j.chemgeo.2013.09.019

Prasad, A. S., Bao, B., Beck, F. W. J., Kucuk, O., and Sarkar, F. H. (2004). Antioxidant effect of zinc in humans. *Free Radic. Biol. Med.* 37, 1182–1190. doi: 10.1016/j.freeradbiomed.2004.07.007

Rauch, J. N., and Pacyna, J. M. (2009). Earth's global Ag, Al, Cr, Cu, Fe, Ni, Pb, and Zn cycles. *Gloabal Biogeochem Cycles* 23, doi: 10.1029/2008GB003376

Rubasinghege, G., Lentz, R. W., Elzey, S., Baltrusaitis, J., Jayaweera, P. M., Scherer, M. M., et al. (2010). Simulated atmospheric processing of iron oxyhydroxide minerals at low pH: roles of particle size and acid anion in iron dissolution. *Proc. Natl. Acad. Sci. U. S. A.* 107, 6628–6633. doi: 10.1073/pnas.0910809107

Rudnick, R. L., and Gao, S. (2003). Composition of the continental crust. *Treatise on Geochemistry* 3, 1–64. doi: 10.1016/B0-08-043751-6/03016-4

Schleicher, N. J., Norra, S., Chai, F., Chen, Y., Wang, S., Cen, K., et al. (2011). Temporal variability of trace metal mobility of urban particulate matter from Beijing–a contribution to health impact assessments of aerosols. *Atmos. Environ.* 45, 7248–7265. doi: 10.1016/j.atmosenv.2011.08.067

Schleicher, N. J., Norra, S., Chai, F., Chen, Y., Wang, S., and Stüben, D. (2010). Anthropogenic versus geogenic contribution to total suspended atmospheric particulate matter and its variations during a 2-year sampling period in Beijing, China. *J. Environ. Monit.* 12, 434–441. doi: 10.1039/B914739J

Shiel, A. E., Weis, D., and Orians, K. J. (2010). Evaluation of zinc, cadmium and lead isotope fractionation during smelting and refining. *Sci. Total Environ.* 408, 2357–2368. doi: 10.1016/j.scitotenv.2010.02.016

Šillerová, H., Chrastný, V., Vítková, M., Francová, A., Jehlička, J., Gutsch, M. R., et al. (2017). Stable isotope tracing of Ni and Cu pollution in North-East Norway: potentials and drawbacks. *Environ. Pollution.* 228, 149–157.

Sivry, Y., Riotte, J., Sonke, J. E., Audry, S., Schäfer, J., Viers, J., et al. (2008). Zn isotopes as tracers of anthropogenic pollution from Zn-ore smelters The Riou Mort-Lot River system. *Chem. Geol.* 255, 295–304. doi: 10.1016/j.chemgeo.2008.06.038

Sonke, J. E., Sivry, Y., Viers, J., Freydier, R., Dejonghe, L., Andr,é, L., et al. (2008). Historical variations in the isotopic composition of atmospheric zinc deposition from a zinc smelter. *Chem. Geol.* 252, 145–157. doi: 10.1016/j.chemgeo.2008.02.006

Sossi, P. A., Halverson, G. P., Nebel, O., and Eggins, S. M. (2015). Combined separation of Cu, Fe and Zn from rock matrices and improved analytical protocols for stable isotope determination. *Geostand. Geoanal. Res.* 39, 129–149. doi: 10.1111/j.1751-908X.2014.00298.x

Souto-Oliveira, C. E., Babinskia, M., Araújoc, D. F., and Andrade, M. F. (2018). Multi-isotopic fingerprints (Pb, Zn, Cu) applied for urban aerosol source apportionment and discrimination. *Sci. Total Environ.* 626, 1350–1366. doi: 10.1016/j.scitotenv.2018.01.192

Souto-Oliveira, C. E., Babinskia, M., Araújoc, D. F., Weiss, D. J., and Ruiz, I. R. (2019). Multi-isotope approach of Pb, Cu and Zn in urban aerosols and anthropogenic sources improves tracing of the atmospheric pollutant sources in megacities. *Atmos. Environ.* 198, 427–437. doi: 10.1016/j.atmosenv.2018.11.007

Sun, Y., Zhuang, G., Huang, K., Li, J., Wang, Q., Wang, Y., et al. (2010). Asian dust over northern China and its impact on the downstream aerosol chemistry in 2004. *J. Geophys. Res.* 115:D00K09. doi: 10.1029/2009JD012757

Taylor, S. R., and McLennan, S. M. (1985). *The Continental Crust: Its Composition and Evolution*. Blackwell: Cambridge.

Thapalia, A., Borrok, D. M., Van Metre, P. C., Musgrove, M., and Landa, E. R. (2010). Zn and Cu isotopes as tracers of anthropogenic contamination in a sediment core from an urban lake. *Environ. Sci. Technol.* 44, 1544–1550. doi: 10.1021/es902933y

Uno, I., Eguchi, K., Yumimoto, K., Takemura, T., Shimizu, A., Uematsu, M., et al. (2009). Asian dust transported one full circuit around the globe. *Nat. Geosci.* 2, 557–560. doi: 10.1038/ngeo583

Vance, D., Archer, C., Bermin, J., Perkins, P. J., Statham, P. J., Lohan, M. C., et al. (2008). The copper isotope geochemistry of rivers and the oceans. *Earth Planet. Sci. Lett.* 274, 204–213. doi: 10.1016/j.epsl.2008.07.026

Voldrichova, P., Chrastny, V., Sipkova, A., Farkas, J., Novak, M., Stepanova, M., et al. (2014). Zinc isotope systematics in snow and ice accretions in Central European mountains. *Chem. Geol.* 388, 130–141. doi: 10.1016/j.chemgeo.2014.09.008

Wang, Z.-Z., Liu, S.-A., Liu, J., Huang, J., Xiao, Y., Chu, Z.-Y., et al. (2017). Zinc isotope fractionation during mantle melting and constraints on the Zn isotope composition of Earth's upper mantle. *Geochim. Cosmochim. Acta* 198, 151–167. doi: 10.1016/j.gca.2016.11.014

Weiss, D. J., Kober, B., Gallagher, K., Dolgopolova, A., Mason, T. F. D., Coles, B. J., et al. (2004). Accurate and precise Pb isotope measurements in environmental samples using MC-ICP-MS. *Intern. J. Mass Spectrom.* 232, 205–215. doi: 10.1016/j.ijms.2004.01.005

Werner, R. A., and Brand, W. A. (2001). Referencing strategies and techniques in stable isotope ratio analyis. *Rapid Commun. Mass Spectrom.* 15, 501–519. doi: 10.1002/rcm.258

Wiederhold, J. G. (2015). Metal stable isotope signatures as tracers in environmental geochemistry. *Environ. Sci. Technol.* 49, 2606–2624. doi: 10.1021/es504683e

Xie, S., Yu, T., Zhang, Y., Zeng, L., Qi, L., and Tang, X. (2005). Characteristics of PM10, SO2, NOx and O3 in ambient air during the dust storm period in Beijing. *Sci. Total Environ.* 376, 100–108. doi: 10.1016/j.scitotenv.2004.10.013

Xuan, J., and Sokolik, I. N. (2002). Characterization of sources and emission rates of mineral dust in Northern China. *Atmos. Environ.* 36, 4863–4876. doi: 10.1016/S1352-2310(02)00585-X

Yan, Y., Sun, Y. B., Weiss, D., Liang, L. J., and Chen, H. Y. (2015). Polluted dust derived from long-range transport as a major end member of urban aerosols and its implication of non-point pollution in northern China. *Sci. Total Environ.* 506, 538–545. doi: 10.1016/j.scitotenv.2014.11.071

Yang, Y., Zhang, X., Liu, S.-A., Zhou, T., Fan, H., Yu, H., et al. (2018). Calibrating NIST SRM 683 as a new international reference standard for Zn isotopes. *J. Anal. At. Spectrom.* 33, 1777–1783. doi: 10.1039/C8JA00249E

Yin, N.-H., Sivry, N., Benedetti, M. F., Lens, P. N. L., and van Hullebusch, E. D. (2016). Application of Zn isotopes in environmental impact assessment of Zn-Pb metallurgical industries: a mini review. *Appl. Geochem.* 64, 128–135. doi: 10.1016/j.apgeochem.2015.09.016

Yin, N.-H., van Hullebusch, E. D., Benedetti, M., Lens, P. N. L., and Sivry, Y. (2018). Zn isotopes fractionation during slags' weathering: one source of contamination, multiple isotopic signatures. *Chemosphere* 195, 483–490. doi: 10.1016/j.chemosphere.2017.11.184

Yu, Y., Norra, S., Schleicher, N., Fricker, M., Dietze, V., Kaminski, U., et al. (2011). Dynamics and origin of PM2.5 during a 3-year sampling period in Beijing, China. *J. Environ. Monit*. 13, 334–346. doi: 10.1039/C0EM00467G

Zhang, R., Russell, J., Xiao, X., Zhang, F., Li, T., Liu, Z., et al. (2018). Historical records, distributions and sources of mercury and zinc in sediments of East China sea: implication from stable isotopic compositions. *Chemosphere* 205, 698–708. doi: 10.1016/j.chemosphere.2018.04.100

Zhao, Y., Vance, D., Abouchami, W., and de Baar, H. J. W. (2014). Biogeochemical cycling of zinc and its isotoopes in the Southern Ocean. *Geochim. Cosmochim. Acta* 125, 653–672. doi: 10.1016/j.gca.2013.07.045

Zhu, X. K., Guo, Y., Williams, R. J. P., O'Nions, R. K., Matthews, A., Belshaw, N. S., et al. (2002). Mass fractionation processes of transition metal isotopes. *Earth Planet. Sc. Lett*. 200, 47–62. doi: 10.1016/S0012-821X(02)00615-5

Conflict of Interest: SD was employed by company Agilent Technologies Co. Ltd, China.

The remaining authors declare that the research was conducted in the absence of any commercial or financial relationships that could be construed as a potential conflict of interest.